PRODUCTION AND CHARACTERIZATION OF HEAT INSULATING PANELS

A Thesis Submitted to
the Graduate School of Engineering and Sciences of
Izmir Institute of Technology
in Partial Fulfillment of the Requirements for the Degree of

MASTER OF SCIENCE

in Chemical Engineering

by
Osman Giray YÖRÜK

October 2016
İZMİR

We approve the thesis of **Osman Giray YÖRÜK**

Examining Committee Members:

Assoc. Prof. Dr. Ekrem ÖZDEMİR
Department of Chemical Engineering, Izmir Institute of Technology

Prof. Dr. Selahattin YILMAZ
Department of Chemical Engineering, Izmir Institute of Technology

Assoc. Prof. Dr. Serap CESUR
Department of Chemical Engineering, Ege University

26 October 2016

Assoc. Prof. Dr. Ekrem ÖZDEMİR
Supervisor, Department of Chemical Engineering
Izmir Institute of Technology

Prof. Dr. Fehime ÇAKICIOĞLU ÖZKAN
Head of the Department of Chemical School of Engineering

Prof. Dr. Bilge KARAÇALI
Dean of the Graduated Engineering and Sciences

ACKNOWLEDGEMENTS

I express my deep gratitude to my advisor Assoc. Prof. Dr. Ekrem ÖZDEMİR for his guidance and help throughout this thesis. I would like to thank for his understanding, constantly invaluable guidance and knowledge in every stage of my thesis study.

I would also thank Prof. Dr. Lütfi ÖZYÜZER at the Physics Department for his guidance on preparation of the film coating and characterization of vacuum insulating panels.

I thank Elif Nur HAYTA for her warm friendship and technical support. I also thank Mehmet Ziya OKUR, Yücel AYDOĞAN, Hasan ÖRTÜN, Mehmet Salih YILDIZ, Gülşah KÜRKÇÜ, Umur AYAZ Gazi ÖZDEMİR, Gülsüm SEZİŞ, Meryem DENİZ, and Serpil ÇELİK.

To my wonderful family – Mom and Dad, Alim, Zehra. They have always been with me, every step of the way, and I express my heartfelt gratitude for their unconditional love, support, encouragement, and instilling in me the belief that I could do anything I put my mind to.

This project was funded by the Ministry of Science, Industry, and Technology (BSTB) through the project number of SAN-TEZ 0521.STZ.2013-2, and I would like to thank BSTB for the financial support.

Also, the hollow nano calcite particles were synthesized with the process developed in a project funded by the Scientific and Technological Council of Turkey (TUBITAK) with a project number of 110M104, and I would like to thank TUBITAK for financial support.

ABSTRACT

PRODUCTION AND CHARACTERIZATION OF HEAT INSULATING PANELS

Hollow nano calcite particles were used as a core material in vacuum insulation panels (VIPs) and compared it with the fumed silica generally used in VIPs as the core material. Zinc-Tin-oxide (ZTO), $ZnSnO_x$, was coated on the polyamide/polyethylene (PA/PE) polymeric films and used as the barrier material in VIPs to prohibit moisture and air transport. A fluidized bed filtration system was developed to separate the produced hollow nano particles from its slurry. $ZnSnO_x$ coating on the PA/PE polymeric films were optimized with respect to film rotation rate and oxygen content during film coating. Water permeation rate was measured as 8.32 $gday^{-1}m^{-2}$ for the commercial Aluminum-PET (Al-PET). The water permeation rate was measured as 1.15 $gday^{-1}m^{-2}$ for the 90 μm of PA/PE films coated with ZTO in 500 rpm of film rotation rate and 30 sccm Ar + 7.5 sccm O_2 feed rate. It was shown that the produced ZTO coated PA/PE films had better barrier properties compared to the commercial Al-PET. The thermal conductivity was measured as 8.63 $mWm^{-1}K^{-1}$ for 3 wt% hollow nano calcite in 87 wt% of fumed silica compared to that of 9.9 $mWm^{-1}K^{-1}$ for fumed silica only. It was shown that when 3 wt% of hollow nano calcite were mixed with fumed silica as the core material, better thermal conductivity values were obtained.

ÖZET

ISI YALITIM PANELLERİNİN ÜRETİMİ VE KARAKTERİZASYONU

Vakum izolasyon panelleri (VIP)'nde çekirdek malzeme olarak delikli nano kalsit tanecikleri kullanıldı ve genellikle VIP'lerde kullanılan füme silika ile karşılaştırıldı. Çinko-kalay-oksit (ZTO), $ZnSnO_x$, polyamid/polyetilen (PA/PE) polimerik filmlere kaplandı ve vakum izolasyon panellerinde nem ve hava geçirgenliği için bariyer malzeme olarak kullanıldı. Üretilen delikli nano tanecikleri süspansiyon sıvısından ayırmak üzere bir akışkan yatak filtrasyon sistemi geliştirildi. PA/PE polimerik filmlere $ZnSnO_x$ kaplama filmler sarma hızı ve oksijen miktarı açısından optimize edildi. Su buharı geçiş hızı ticari aluminyum-PET (Al-PET) için 8.32 $ggün^{-1}m^{-2}$ olarak ölçüldü. Su buharı geçiş hızı 500 rpm film sarma hızı ve 30 sccm Ar + 7,5 sccm O_2 besleme kullanılarak çinko-kalay-oksit kaplanmış 90 μm PA/PE filmler için 1.15 $ggün^{-1}m^{-2}$ olarak ölçüldü. Ticari Al-PET ile karşılaştırıldığında üretilen ZTO kaplı PA/PE filmlerin çok daha iyi bariyer özelliğine sahip oldukları gösterildi. Yalnızca füme silika için 9.9 $mWm^{-1}K^{-1}$ olarak ölçülen ısı iletkenlik katsayısı, ağırlıkça %87 füme silika içerisinde %3 delikli nano kalsit için 8.63 $mWm^{-1}K^{-1}$ olarak ölçüldü. Ağırlıkça %3 delikli nano kalsit çekirdek malzeme olarak füme silika ile birleştirildiğinde daha iyi ısı iletkenlik katsayısı değerleri elde edilebileceği gösterildi.

TABLE OF CONTENTS

LIST OF FIGURES

Figure **Page**

LIST OF TABLES

Table **Page**

CHAPTER 1

INTRODUCTION

Vacuum Insulation Panels (VIPs) are one of the most promising energy saving materials need to be used in the near future. Energy is the most demanding source in our society and its usage has been increasing since the industrial revolution (Alotaibi and Riffat 2014). The future predictions show that the energy usage will increase even faster. The population of the earth has been increasing from 6 billion in 1930s and projected to increase to 9.1 billion in 2050s. The energy consumption has been increasing in parallel to the population. As a consequence, the carbon dioxide (CO_2) release to the atmosphere has been increasing since the industrial revolution. For instance, the atmospheric concentration of CO_2 has been increased from 280 ppm in 1930 to 403 ppm in 2016. Therefore, consumption of energy is directly related to the environmental pollution. Because, energy is expensive, the loss of energy is important and need to be preserved. Any technology developed for preventing the energy loss will help saving our planet and create an economic incentive. Therefore, most efficient energy insulation tools, which were mostly used in refrigerators, coolers, trucks etc., as shown in Figure 1.1, need to be developed, for which one of the most important example is a VIP.

Figure 1.1. Places where the most energy savings needed are refrigerators, coolers, trucks etc..

A VIP consists of a core material under vacuum and a protective barrier to inhibit gas and moisture transport to the core material. Figure 1.2 shows a picture of a VIP with its core and barrier materials. Core material is used for heat insulation and the barrier material is used for a vacuum entrapment. The VIPs are thin materials compared to its counterparts.

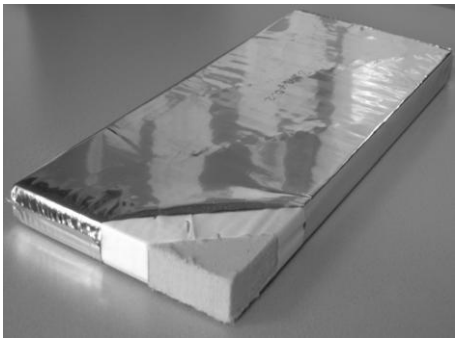

Figure 1.2. A picture of vacuum insulation panel (VIP) with its core and barrier materials

Figure 1.3 shows different heat insulation materials such as cork, expanded polystyrene (EPS), glass fibers, extruded polystyrene (XPS) and polyurethane. As shown from the picture in Figure 1.3(a), the thickness of these materials is considerably higher than the VIPs. The thermal conductivity values were compared for the alternative heat insulation materials in Figure 1.3(b). The thicknesses of the required heat insulators are also compared in Figure 1.3(b) for the same heat resistance of 5 $m^2KW^{-1}cm^{-1}$. As shown in the figure, the VIP is the thinnest material among its other counterparts.

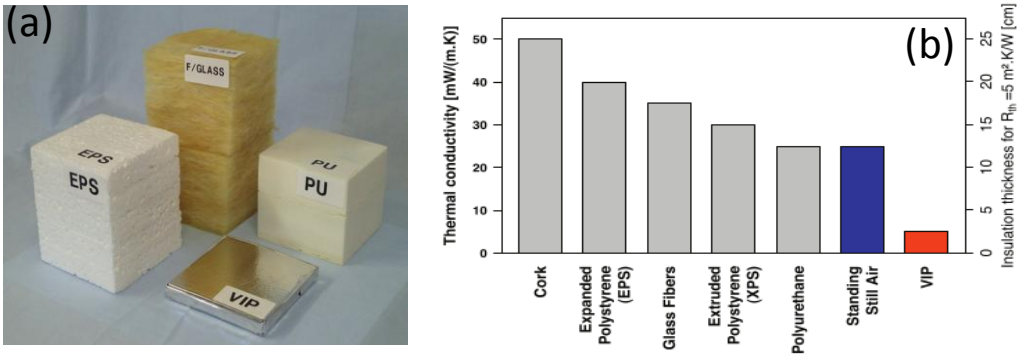

Figure 1.3. Comparison of the thickness and thermal conductivity of different insulation materials (a) picture for the thicknesses for the same thermal conductivity and (b) values for the thermal conductivity and insulation thicknesses (Source: Bouquerel, Duforestel et al. 2012).

Thermal conductivity of VIPs varies with vacuum pressures. As can be seen in Figure 1.4, the thermal conductivity of different core materials decreases as the vacuum pressure decreases. Again, the fumed silica shows a better performance since the thermal conductivity of the VIP is lower at relatively higher vacuum pressures. Higher vacuum pressures are needed for the other core materials in order to obtain similar thermal conductivity values.

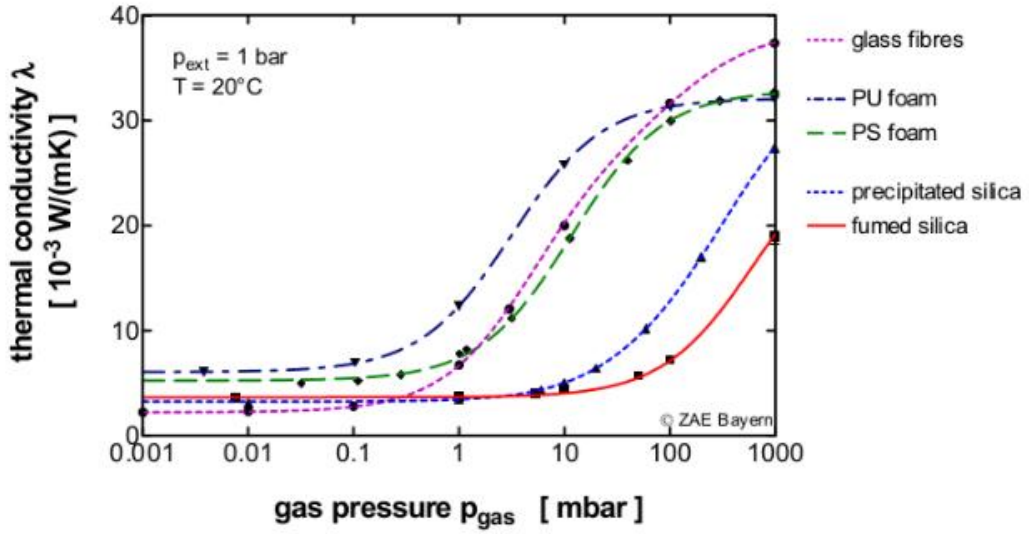

Figure 1.4. Thermal conductivity of VIPs with different core materials as a function of vacuum pressures (Source: Bouquerel, Duforestel et al. 2012)

A porous material can be selected for a core material for better heat insulation panel. Effect of pore diameter of a core material in VIPs as a function of vacuum pressures was shown in Figure 1.5. As shown in the figure, when the pore diameter was smaller, better performance can be obtained at relatively higher vacuum pressures for the VIPs. It can be concluded that the porous core materials could be a good candidate for VIPs.

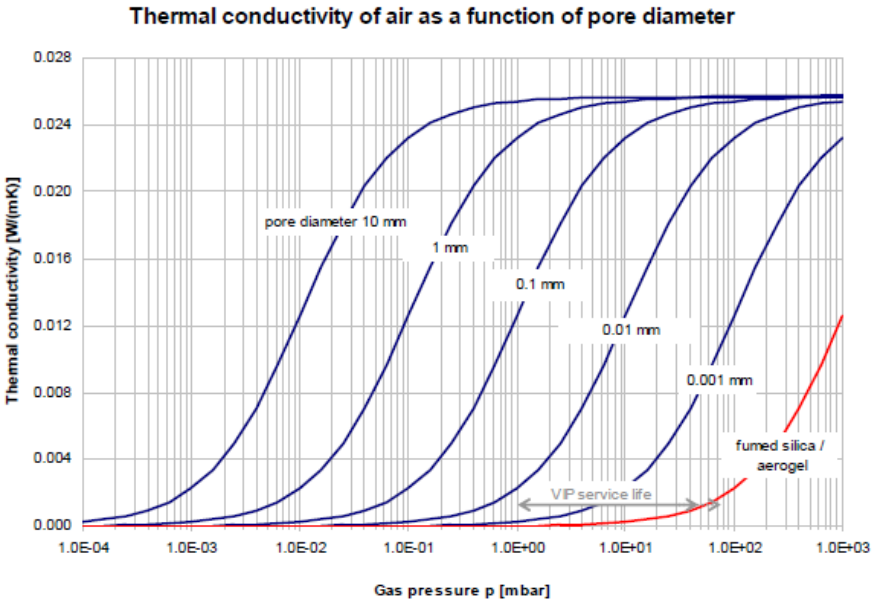

Figure 1.5. Effect of pore diameter of a core material in VIPs as a function of vacuum pressures (Source: Bouquerel, Duforestel et al. 2012)

However, keeping the vacuum in VIPs is an important parameter for their stability and longer life times. Polymeric barrier materials can be used to protect the water vapor transfer rate (WVTR) and air transfer rate (ATR) to the VIPs. Because the pressure is lower than the ambient pressure in VIPs, as shown in Figure 1.6, moisture and air can diffuse into a VIP. The water and air can also diffuse through the joints in the barrier materials. Barrier materials with poor moisture and air transport properties need to be developed in order to keep the vacuum in the VIPs and extend their life time for their usage.

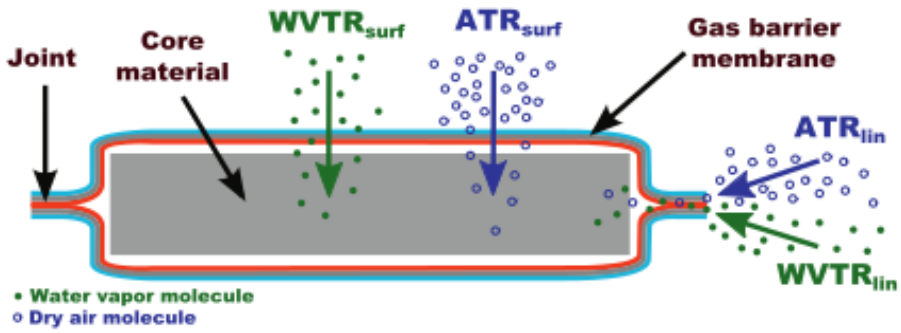

Figure 1.6. Barrier in VIPs for moisture and air transport. Here, WVTR: water vapor transport rate, ATR: air transport rate (Source: Alotaibi and Riffat 2014).

Some oxide forms of metals were shown in Figure 1.7 for the water vapor transfer rates through a polymeric film barrier. As can be seen from the figure, zinc-tin-oxide (ZTO), $ZnSnO_x$, was found to be the best oxide polymer film for the lower water vapor transport rate (WVTR). Titanium oxide (TiO_2) seems to perform worse for the water transport in VIPs. Therefore, $ZnSnO_x$ was thought to be one of the coating materials on the polymeric barriers in VIPs.

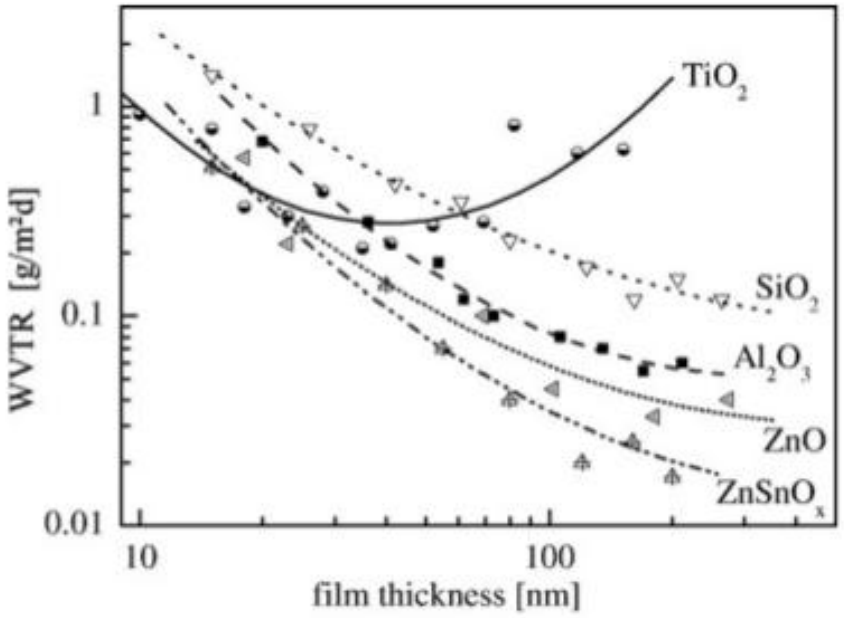

Figure 1.7. Effect of different oxides on the water vapor transfer rate (WVTR) as a function of coated film thickness on polymeric film barriers (Source: Sato, Kiyohara et al. 2009).

The core material can be powder, porous foam, hollow spheres, and high surface area fibers. Among these, fumed silica has been employed extensively in VIPs. However, there are some disadvantages using the fumed silica as the core material in VIPs. For instance, fumed silica is expensive, it is not produced nationally and generally exported from overseas, and its light-weight density cause the panels poor in mechanical strength. Thus, alternative core materials need to be developed in order to decrease the product cost and to increase the performance of VIPs for a better energy protection.

Alumina-PET (Al-PET) has been used as the protective barrier for the VIPs. Al-PET is a good barrier for oxygen and moisture transport and can be obtained from the

market easily. However, Al-PET forms a thermal bridge in VIPs, which increases the heat transport (Alotaibi and Riffat 2014). Therefore, better insulating materials need to be developed.

In a study, conducted by our group with a research project funded by The Scientific and Technological Research Council of Turkey (TUBITAK) with a project number of 110M104, a method was developed to synthesize hollow nano calcite ($CaCO_3$) particles with homogenous size distribution. It was proposed that these nano particles of sizes less than 350 nm and a pore size of less than 40 nm can be a good candidate as a core material in VIPs. Also, as shown in Figure 1.7, the $ZnSnO_x$ has a lower water permeability, and low thermal conductivity due to its oxide form (Sato, Kiyohara et al. 2009). It was also proposed that $ZnSnO_x$ could be a good candidate for the barrier material on the VIPs. Therefore, it was aimed in this Master Thesis to use hollow nano calcite particles as the core material and $ZnSnO_x$ coated PA/PE polymeric films as a barrier for VIPs. Better thermal conductivity values were expected to obtain for the new design VIP compared to those in which fumed silica is used as the core material.

CHAPTER 2

BACKGROUND AND LITERATURE REVIEW

2.1 Calcium Carbonate

Calcium carbonate ($CaCO_3$) consists of three elements carbon, oxygen and calcium with the formula of $CaCO_3$. It is a natural mineral found in rocks, mostly limestone, and is the main component of mollusk shells, egg shells, pearls, and snails (Al Omari, Rashid et al. 2016). $CaCO_3$ is a commonly studied substrate due to importance of its precipitation either in nature or industry. For instance, biological $CaCO_3$ production of organisms in deep sea is crucial for the CO_2 and calcium balances (Peterson, 2001). $CaCO_3$ is also industrially employed as filler material for paper, rubber, paints, plastics, adhesives and other materials for many years (Chen and Xiang 2009). Controlling $CaCO_3$ precipitation is important because its undesired precipitation causes problems in heat exchangers and it is among the important scale-forming minerals in oil and gas production pipelines (Flaten, Seiersten et al. 2009). Understanding nucleation and particle growth to control $CaCO_3$ formation is crucial. Some ofthe physical properties of calcium carbonate are summarized in Table 2.1.

Table 2.1. Physical properties of calcium carbonate (Source: Flaten, Seiersten et al. 2009)

Physical Properties	
Molecular weight	100.09 daltons
Surface area (BET)	20-35 m^2/g
Refractive index at 25 °C	1.48, 1.65
Density at 20 °C	2710 kg/m^3
Thermal conductivity at 25 °C	2.6 W/m. K
Solubility in water at 25 °C	0.013 g/L

Polymorphism of calcium carbonate: $CaCO_3$ exists in six solid forms. Three of them are hydrated which are called as amorphous calcium carbonate (ACC),

monohydrate calcium carbonate (MCC) and hexahydrate calcium carbonate (HCC) have higher solubility in water (Andreassen 2001). Anhydrous forms of $CaCO_3$ are called as vaterite, aragonite and calcite, with hexagonal, orthorhombic and rhombohedral structures, respectively (Hadiko, Han et al. 2005). Thermodynamically the most stable form of polymorphs under ambient conditions is calcite and it is the most abundant form of $CaCO_3$ in nature. Difference of growth and nucleation rate of various polymorphs effects the abundance of polymorphs. Calcite is the least soluble in water. Differences of solubility and stability of polymorphs cause the precursors to dissolve and transform to calcite (Andreassen 2001, Hadiko, Han et al. 2005).

Vaterite is the least stable form of calcium carbonate polymorphs under ambient conditions. But, due to its biological activities, it has been widely studied. There are two main methods for vaterite formation. One is mixing calcium salt and carbonate solution and the other is to pass CO_2 gas through calcium salt solution. Vaterite is synthesized at ambient temperature by reaction of CO_2 with an aqueous solution of calcium chloride ($CaCl_2$) in the presence of ammonia (Hadiko, Han et al. 2005). Han, Hadiko (Han, Hadiko et al. 2006) concluded that vaterite formation can be obtained by precipitation at low pH. Throughout the precipitation, ammonia was added to the solution to keep pH at low values and ammonia addition resulted in increase of supersaturation and formation of more nuclei, which enhances vaterite nuclei growth and suppresses vaterite transformation into calcite.

The crystal structure of vaterite is hexagonal but it precipitates as spheres (Andreassen 2001). SEM image of vaterite crystals is given in Figure 2.1.

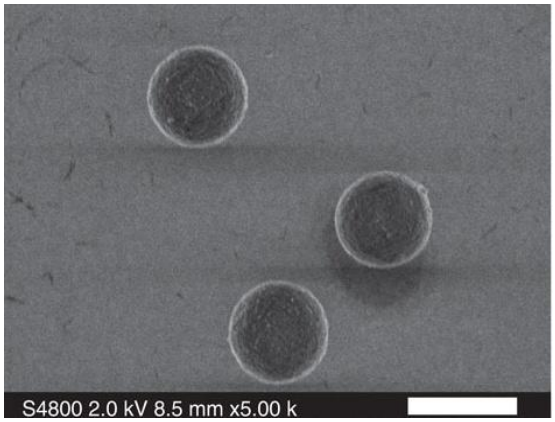

Figure 2.1. SEM image of vaterite particles, scale bar is 5µm (Source: Arita, Mazilu et al. 2013)

Aragonit particles are needle-like shaped and have orthorhombic structure. They precipitate as single needles or rosettes of radiating needles(Andreassen 2001). SEM image of aragonite crystals is given in Figure 2.2. Aragonite crystals are produced by mixing of solutions method, slow Na_2CO_3 addition in Kraft pulping (Konno, Nanri et al. 2003). Chen and Tai (Chang and Tai 2010) produced aragonite crystals in a fluidized-bed crystallizer under magnetic field effect and concluded that magnetic field application induces the aragonite growth and suppress calcite growth. Lower pH environment causes faster aragonite crystal growth. Moreover, Andreassen (Andreassen 2001) stated that the growth rate of aragonite is highly temperature dependent and the aragonite particles are more stable at higher temperatures.

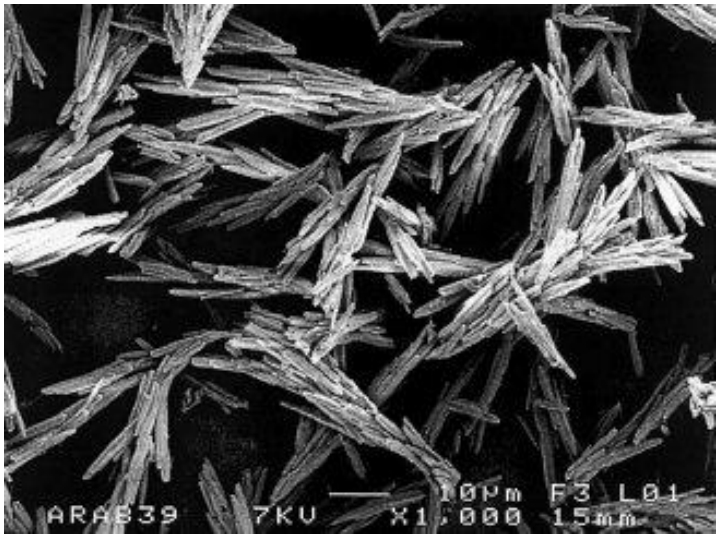

Figure 2.2. SEM image of aragonite crystals (Source: Lucas-Girot, Verdier et al. 2005)

Calcite is the thermodynamically most stable polymorph of calcium carbonate under ambient conditions. It is hexagonal shaped and has a rhombohedral structure (Andreassen 2001). SEM image of calcite particles is given in Figure 2.3. Aragonite and vaterite which are unstable forms of $CaCO_3$ can transform into calcite which is stable form under ambient conditions. Temperature, initial concentrations and additives affect the polymorphism (Andreassen 2001, Chen and Xiang 2009).

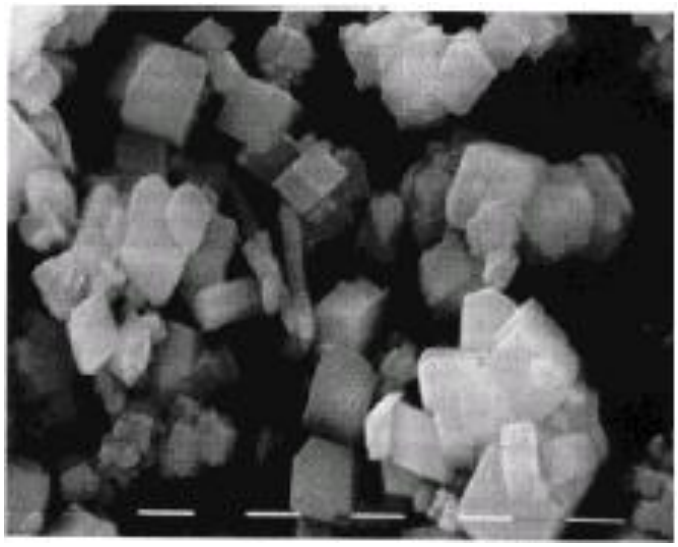

Figure 2.3. SEM image of calcite particles (Source: Söhnel and Garside, 1992)

Calcite Production Methods: Calcite production methods can be classified as chemical method and carbonization method. The chemical method is divided into two processes called solution method and Kraft method. In solution method, calcium (Ca^{++}) ion source is calcium chloride ($CaCI_2$) and carbonate ($CO_3^{=}$) ion source is sodium carbonate (Na_2CO_3). They are mixed at certain conditions to form calcite (Wray and Daniels 1957, Rieger, Thieme et al. 2000, Pontoni, Bolze et al. 2003). Wray and Daniels (Wray and Daniels 1957) reported the batch technique which is the addition of $CaCl_2$ solution into certain amount of Na_2CO_3 in a batch reactor. In double-jet technique, Na_2CO_3 and $CaCl_2$ solutions are simultaneously pumped into the reactor. In Kraft method, Ca^{++} ion source is calcium hydroxide ($Ca(OH)_2$) and $CO_3^{=}$ ion source is Na_2CO_3 and certain amounts of the reactants are mixed (Konno, Nanri et al. 2003). Although the parameters effecting crystallization morphology can easily be controlled in chemical method, it is hard to control the nucleation and crystal grow rates. Moreover, the size of the particles produced by chemical method is larger than 2 micron. Thus, chemical method is not proper for production of nano-sized calcite particles at industrial scale (Kralj, Brečević et al. 1997, Hadiko, Han et al. 2005, Han, Hadiko et al. 2006, Lopez, Zuddas et al. 2009).

Carbonization method is commonly used for nano $CaCO_3$ production at industrial scale due to its cheap and availability in raw materials. In this method, CO_2 gas is passed through aqueous slurry of slaked lime ($Ca(OH)_2$ suspension in a batch or semi-batch process (Uebo, Yamazaki et al. 1992, García-Carmona, Morales et al. 2003,

Garcí, Morales et al. 2004, Ukrainczyk, Kontrec et al. 2007). $Ca(OH)_2$ solution or lime slurry prepared at desired concentration is fed into crystallization tank and stirred. The pH and conductivity values are adjusted by $Ca(OH)_2$ or CO_2 feed rates. When the pH deceased to 7.0, the reaction is terminated. The temperature is kept constant during crystallization. At the end, solid nano $CaCO_3$ particles are separated and analyzed.

Applications of Calcium Carbonate: $CaCO_3$ is widely employed in various industries such as oil, paint, paper, plastics, coatings as filling material (Hadiko, Han et al. 2005). Furthermore, $CaCO_3$ is used in environmental friendly items, calcium enriched foods, drug delivery vehicles, templates for microcapsules (Render, Samuel et al. 2016). Usage of calcite as the most stable polymorph of $CaCO_3$ for production of polymeric composite materials has been reported by many researchers (Chan, Wu et al. 2002, Guo, Yu et al. 2006, Liang 2007, Lin, Chen et al. 2008, Hu, Dong et al. 2009, Gao 2012). In polymeric composites, calcite usage has enhanced the tensile strength and Young's modulus (Guo, Yu et al. 2006, Liang 2007, Hu, Dong et al. 2009). Among these various application areas, the calcite is used in this study as a core material in vacuum insulation panels.

2.2 Vacuum Insulation Panels (VIPs)

A VIP is a thermal insulation material containing a core material and a barrier envelope as shown in Figure 2.4. The main components of a VIP are inner core, barrier envelope, getters or desiccants and opacifiers as the schematic view of a VIP is given in Figure 2.5. Generally, two types of layers such as thick metal sheets or multilayer barrier of polymeric layers are used in outer envelope to provide inner core material against the gas diffusion and mechanical damage. Durability of VIPs is a crucial feature. VIPs withstand mechanical and environmental stresses over their design service life which is more than about 10 years for commercial applications. Any small pinhole or damage leads to the loss of thermal insulation ability and failure of VIP (Tenpierik and Cauberg 2010).

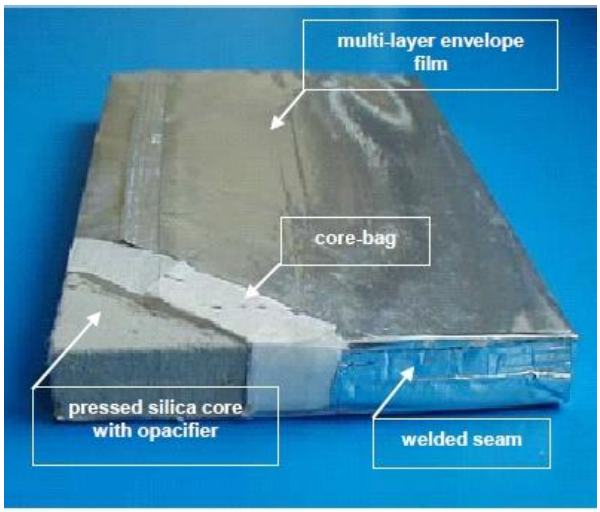

Figure 2.4. A vacuum insulation panel (Source: Heineman, Schwab et al. 2005, Simmler and Brunner 2005)

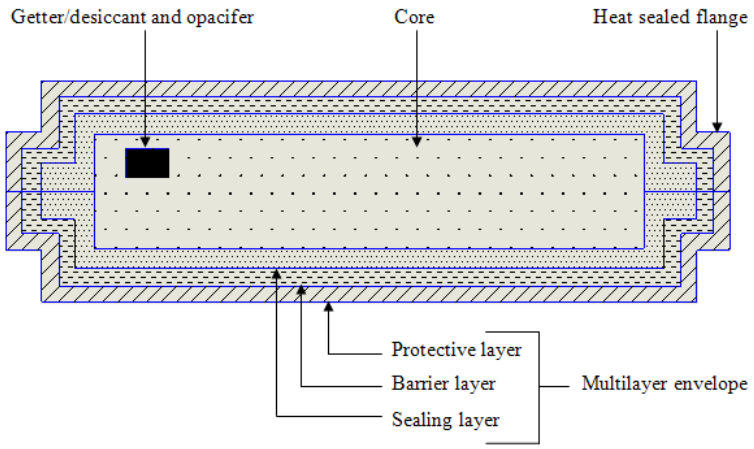

Figure 2.5. Schematic of a VIP (Source: Alam, Singh et al. 2011)

Foil based VIPs are made with metal sheet envelope welded into one piece around evacuated core. These VIPs demonstrate superior load bearing capacity and resistance to mechanical damage. Metal sheet envelopes offer great resistance to water vapor and gas diffusion. However, these VIP envelopes contribute a greater thermal bridging effect and will reduce the overall thermal performance of VIPs (Willems, Schild et al. 2005, Willems 2005). Polymeric film based VIPs are made with laminates of metallized polymeric films. These films are coated with metal oxides with thickness in the range of 100-150 μm to improve the barrier properties for the water vapor permeability and gas diffusion. Contrary to sheet based VIPs, contribution of polymeric

film based envelopes to thermal edge effect and weight is minimal. However, these barrier envelops provide shorter service life and prone to damage during installation.

Structure of vacuum insulation panels:

Core materials: The core of a VIP consists of porous materials such as open porous foams, powders and fibers with appropriate pore size. The duty of the core material is physically supporting the VIP envelope against atmospheric pressure after evacuation, reducing radiative heat transfer and establishing spaces that are smaller or in the same order of size as the mean free path length of gas molecule present in the pores. Evacuation process suppresses gaseous heat transfer within the core. Main findings of some research studies examining different materials as core material is given in Table 2.2.

Table 2.2. Thermal conductivities of different core materials

Core material	Main findings	Authors
Organic Melamine-formaldehyde fiber fleece	λ = 2.3 $mWm^{-1}K^{-1}$, density: 250 kgm^{-3}	(Nemanič and Žumer 2015)
Fumed silica kernel	λ = 4 $mWm^{-1}K^{-1}$ below 1 mbar pressure	(Fricke, Schwab et al. 2006)
Polystyrene-Poylethylene core material with carbon black, and calcium stearate	λ = 4.4 - 9.0 $mWm^{-1}K^{-1}$ at 10^{-4}torr	(Tseng and Chu 2009)
Phenolic foam	λ = 5 $mWm^{-1}K^{-1}$ below 0.01 mbar	(Kim, Lee et al. 2012)
Glass fiber chopped strand Glass wool	λ=1.5 $mWm^{-1}K^{-1}$ at inner pressure below 0.1 mbar λ = 2.8 $mWm^{-1}K^{-1}$ at inner pressure below 0.1 mbar	(Di, Gao et al. 2014)
Granular silica	λ = 14 $mWm^{-1}K^{-1}$at 0.1 mbar at density of 130 $kgm^{-3}$when granules were compressed with 1 bar pressure.	(Karami, Afriyie et al. 2014)
Glass fiber	λ = 2-3 $mWm^{-1}K^{-1}$	(Li, Duan et al. 2013)
Open pore melamine - formaldehyde rigid foam	λ = 6 $mWm^{-1}K^{-1}$	(Nemanič, Zajec et al. 2014)

Heat conduction in solid, gas, and any radiation due to temperature occurring in conventional insulation materials are shown in Figure 2.6. As shown in the figure, the total heat transfer in conventional insulation materials such as mineral wool, glass wool or organic foams is dominated by the contribution of the gas within the hollow spaces or pores (Bouquerel, Duforestel et al. 2012). Improvement of insulation material can be achieved by reducing the pressure by evacuating the gas from the pore spaces and eliminating the gas conductivity within the VIPs.

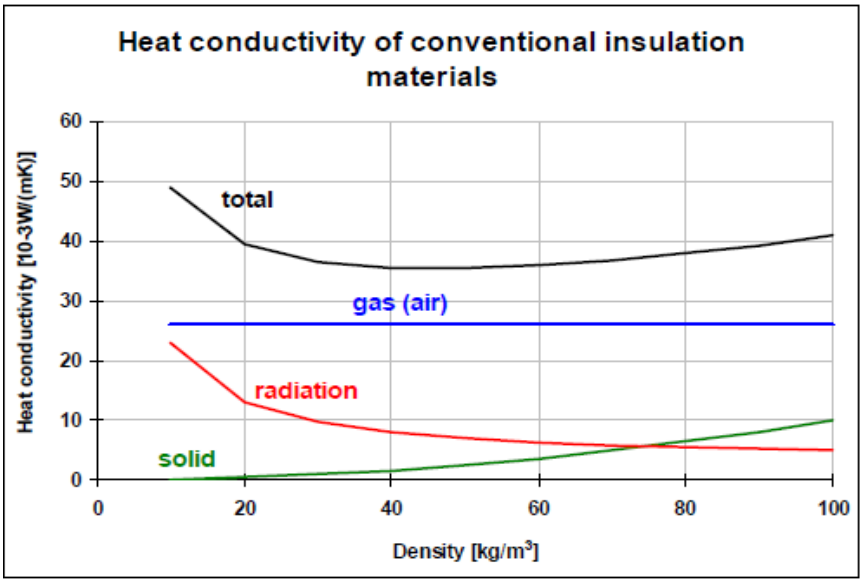

Figure 2.6. Heat conductivity of conventional insulations (fibers and foams) dominated by the gas conductivity (Source: Bouquerel, Duforestel et al. 2012)

Powders such as fumed silica or pyrogenic silica, silica aerogels and expanded perlite are commonly used in the VIP cores. Fumed silica is the most commonly used core material in VIPs due to its low density, high specific surface area and low thermal conductivity. Fumed silica was first developed by Degussa AG (currently Evonik Industries) in Germany in 1942 by the combustion of silicon tetrachloride in an oxygen-hydrogen flame (Evonik Industries, 2006). This process yields molten particle of silicon dioxide. These particles fuse with each other to form chain-like aggregates with mean aggregate size of 0.2-0.3 μm. Fumed silica has low thermal conductivity 3-6 $mWm^{-1}K^{-1}$ at a pressure in the range of 20-100 mbar due to low density, high porosity, small pore size and a specific surface area in the range of 5-60 x 10^{-2} m^2kg^{-1}(Wang, Walliman et al. 2007). The disadvantages of fumed silica are its low resistance to radiative heat transfer and its higher costs (Caps, Fricke et al. 1984).

Silica aerogels, developed by Kistler in 1931 (Kistler and Caldwell 1934), are nano porous materials with pore size of about 20nm, agglomeration size of 1 μm, and bulk density in the range of 3 kg m^{-3} to 350 kg m^{-3}. Silica aerogel is a convenient core material for VIPs due to its low density and small pore size (1-100 nm). The thermal conductivity of Render silica aerogel is about 1-3 $mWm^{-1}K^{-1}$ under vacuum; it is non-reactive and non- flammable (Baetens, Jelle et al. 2011).

Glass fiber can be used as core material and binding material for VIPs which used high temperature application because of low density and high thermal stability (>1000 ^{o}C) (Boafo, Chen et al. 2014). Radiative conductivity of glass fiber was reported to be about 7 $mWm^{-1}K^{-1}$and a solid conductivity of about 2.1 $mWm^{-1}K^{-1}$ with a density of 250 $kg.m^{-3}$ and a fiber diameter of approximately 0.5-0.7 μm at 300 K. Also, overall thermal conductivity of glass fiber was measured as 2.8 $mWm^{-1}K^{-1}$. Some articles give different information of the glass fiber thermal conductivity for core material of VIPs. Nevertheless, a very low pressure of 0.01 mbar is required to suppress the gaseous thermal conductivity to a negligible level (Swimm, Reichenauer et al. 2009). Kwon and Jang (Kwon, Jang et al. 2009) also reported a total theoretical total thermal conductivity value of 3.6 $mWm^{-1}K^{-1}$ for glass fiber core at 0.1 mbar. Araki et al. (Araki, Kamoto et al. 2009) investigated the performance of glass fiber based VIPs for insulating hot water cylinders. Even though, the glass fiber VIPs can achieve a lower initial thermal conductivity compared to fumed silica VIPs, yet these are very sensitive to pressure increase due to their large pore size and moisture content.

Fiber-powder composites are other suitable core material and they can potentially be used as core material in VIPs. Mukhopadhyaya *et al.* (Mukhopadhyaya, Kumaran et al. 2009) suggested the layered composite of glass mineral oxide fiber and wood fiber with pumice and zeolite powders as alternative low cost VIP core materials. Composite layers of fiber and powder boards were placed on top of each other in order to decrease the thermal conductivity and the pore size. Main disadvantage of such composites was their high density ranging from 320-340 kgm^{-3} compared to other core materials. Fiber-powder was found to be comparable to precipitated silica and nanogelsat low pressures of 0.1-1 mbar. However, upon increasing the pressure, the exponential rise in thermal conductivity suggest that pore sizes were not effectively reduced by alternate layering method.

VIP envelope: The external cover of a VIP is called as envelope. The envelop prevents in flux of gases inside the panel. Hence, it provides mechanical strength throughout transportation and installation. The most important features of barrier envelope are low thermal conductivity, flexibility, and mechanical stability. Water vapor transmission rate (WVTR), oxygen transmission rate (OTR) and thermal conductivity values are approximately 0.003-0.005 $g.m^{-2}d^{-1}$, 0.001-0.002 $cm^3m^{-2}d^{-1}$ and 0.15-0.30 $Wm^{-1}K^{-1}$, respectively (Simmler and Brunner 2005). Core material and barrier envelope determine the thermal performance of a VIP throughout its service life. Important properties of VIP envelope are lower oxygen and water transmission rates and minimum thermal conductivity. VIP manufacturers want to WVTR of approximately 0.001 $gm^{-2}d^{-1}$ and OTR to be 0.001$cm^3m^{-2}d^{-1}$, which are expected to provide a service life of approximately 30-50 years for building applications (Simmler and Brunner 2005). Metallised polymeric, aluminium foil and steel films are most popular example of envelope to keep vacuum and to prevent moisture inside the core material (Simmler and Brunner 2005, Fricke, Schwab et al. 2006). Compared to conventional thermal isolation materials, VIPs have a long service life. They provide high barrier property and low thermal bridging effect. In spite of their higher barrier properties compared to metalized polymeric envelopes, aluminium foil envelopes have higher thermal conductivity (about 70 $mWm^{-1}K^{-1}$) compared to metalized film envelopes (about 10 $Wm^{-1}K^{-1}$) (Simmler and Brunner 2005, Brunner, Gasser et al. 2006). Also, the metallic layers have some defect such as pinholes lead to a worse barrier property compared to aluminum foils at ambient pressure (Jung, Yeo et al. 2014).

Structure of Envelope: VIP outer envelope consists of an inner sealing layer, a barrier layer and outer protective layer as shown in Figure 2.7. In this figure outer envelope have three aluminized PET films and a high density polyethylene (HDPE) or low density polyethylene (LDPE) are coupled to form an envelope with a proper adhesive such as polyurethane (Alam, Singh et al. 2011). Also a double envelope with a porous core material between the inner and outer envelope was suggested (Kwon, Jang et al. 2010, Jung, Yeo et al. 2014). The system shown in Figure 2.8 was expected to reduce the gas permeation and to increase the service life, but such additional envelope and core material may increase the thickness and the cost of VIP. Thus, high barrier materials in a single envelope should be developed. Jung and Yeo et al.(Jung, Yeo et al.

2014) studied an aluminum foil envelope with an additional layer of aluminum foil excluding the edges. By this way, gas permeation was decreased to zero in coated region without increasing the heat conduction at the edges, but the edges were still permeable, which causes a performance reduction for the VIP.

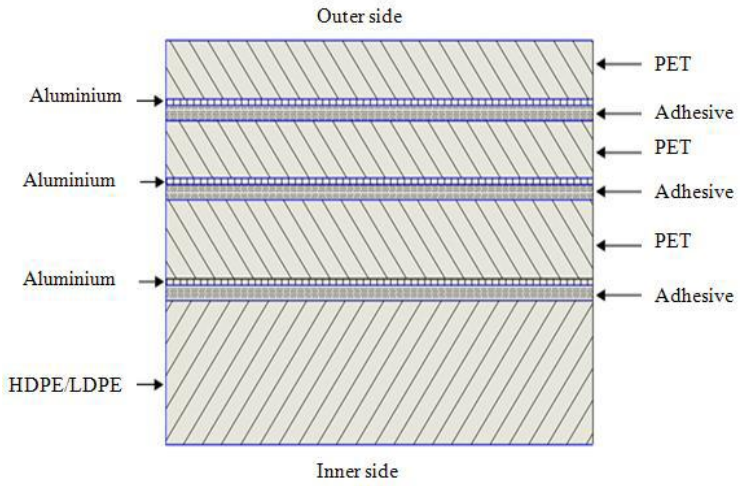

Figure 2.7. Cross section of typical multilayer barrier envelope containing metalized PET layers (Source: Alam, Singh et al. 2011)

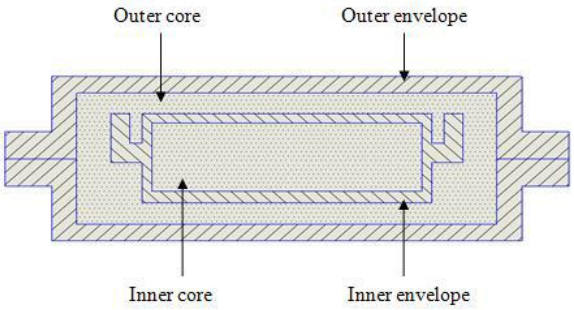

Figure 2.8. Double envelope system (Source: Alam, Singh et al. 2011)

Protective Layer: Protective layer is protecting the VIPs from external stress and supports the barrier layer. It is placed at the outmost layer of the envelope as shown in Figure 2.7. PET, Polypropylene (PP), and polyethylene (PE) are among the polymers which are able to be employed as a protective layer of an envelope. Barrier features of these three polymer films with a thickness of 13 μm at 20 °C and 50% R.H are given in Table 2.3. As shown in the table, WVTR values of PP and PE are very low compared to that of PET. The advantage of using PET as protective layers is its low cost. Other materials are also examined as a possible protective layer. For instance, Araki and

Kamoto et al. (Araki, Kamoto et al. 2009) investigated Polyamide (Nylon 6) to be a protective layer for the VIP envelope for high temperature applications due to its high melting point (225 °C). However, its high cost was a disadvantage for its application. Although barrier properties of protective layer are very important, it is not sufficient for the performance of an envelope. Thus, an additional barrier layer is required.

Table 2.3. Comparison of oxygen and water vapor transmission rates of PET, PP and LDPE (Source: NORNER Industrial Polymer Institute)

Substrate	OTR ($cm^3m^{-2}d^{-1}$)	WVTR($gm^{-2}d^{-1}$)
PET	47.6	7.16
PP	725.9	1.62
LDPE	3215.0	3.29

Barrier Layer: A barrier layer consists of a coating of inorganic material on a polymer substrate. The function of the barrier layer is to prohibit the air and water vapor transmission through the envelope. Coating improves the barrier properties of the layer by one or two orders of magnitude (Alam, Singh et al. 2011). Transparent thin metal oxides such as Silicon oxide (SiO_2), Aluminium oxide (Al_2O_3), Titanium oxide (TiO_2), Zinc oxide (ZnO), Zinc-tin-oxide ($ZnSn_xO_y$) and Indium tin oxide (ITO) are mainly used as barrier coatings in various applications such as food packaging, flat panel displays, organic light emitting diodes, and organic solar cells. However, the use of these coatings for VIP envelope application has not been proposed. OTR and WVTRs along with the coating thicknesses of these coatings are shown in Table 2.4. Among these coatings, Al_2O_3 and ZnO coatings become prominent with their high barrier properties and low cost (Henry, Erlat et al. 2001, Alam, Singh et al. 2011, Fahlteich, Schönberger et al. 2011). The fact that mass transfer occurs through the pinholes or defects on the barriers, the number and size of the micro-defects should be minimized in order to improve the barrier properties. The number of barrier layers in a VIP envelope can vary from one to three; though a three-layer structure is widely used due to its better barrier properties against air and water vapor transmission. Currently, PP and PET are being used as substrates. Araki et al. (Araki, Kamoto et al. 2009) investigated the use of multilayer laminate of ethylene vinyl alcohol copolymer (EVOH) and metallized layer of PET with Nylon 6 and HDPE in VIP envelope and found that WVTR and OTR index for this type of envelope were high as compared to the envelope with aluminum foil.

Teniers (2009) reported a better barrier properties of metalized layer of EVOH. However, due to the presence of high thermal conductivity metal in such barrier layers the thermal bridging effect on edges of VIP became dominant. Thermal bridging effect can be reduced by replacing the metalized barrier layer with silicon oxides (SiO_x) and silicon nitride (SiN_x) coatings.

Table 2.4. Oxygen and Water vapor transmission rates along with coating thickness of various oxides

Substrate	Thickness (μm)	Coating	Thickness (nm)	OTR ($cm^3m^{-2}d^{-1}$)	WVTR($gm-^2d^{-1}$)
PET	75	Al_2O_3	280	0.08	0.03
PET	12	AlO_x	14	2.54	0.99
PET	13	SiO_2	170	0.03	7.86
PET	75	SiO_2	240	0.14	0.15
PET	75	TiO_2	340	0.55	0.30
PET	75	ZnO	100	0.13	0.05
PET	75	$ZnSn_xO_y$	310	0.05	0.01
PET	12	ITO	37	0.78	0.10

Sealing Layer: In an envelope formation process, two laminates are joined together by a sealing layer which is the inner most layers in a multi-layered VIP envelope (Figure 2.5). Seal area represents the weakest point of the envelope through which gases can penetrate to the core and degrade the vacuum inside the core. Therefore, seals with maximum strength are required for VIP envelope to perform its function over longer time period. Heat sealing is a commonly used process to join the laminates. In the sealing process, the laminates surfaces are sandwiched between two hot bars and pressure is applied to create a fusion bonding such as an inter-diffusion of macromolecular chains of two polymer surfaces between the two polymer layers of the laminate. The heat sealing parameters such as the temperature and time play an important role for achieving a strong seal (Marouani 2012). Conventionally LDPE and HDPE thicknesses in between 50 and 70 μm have been used in VIPs as a sealing layer (Brunner, Gasser et al. 2006). Araki et al. (Araki, Kamoto et al. 2009) reported the use of other materials such as polybutylene (PBT) and high retort-cast polypropylene (HR-CPP) as sealing layers for high temperature applications. Van Malsen et al. (Van Malsen, Tenpierik et al. 2008) experimentally found no significant difference between

the seal strength of LDPE and HDPE. Hence it is better to use a material which has lower air and water vapor permeability and at the same time provide better seal strength.

Getters and desiccants: Getters and desiccants are integrated inside a core material to extend the life-time of a VIP by continuously adsorbing water vapors (desiccants) and gases (getters) which may penetrate into it through either permeation from the outside environment or via out-gassing of the core and the envelope materials, or both. In the case of silica core VIPs, core itself acts as a desiccant, but for other core materials, a small amount of silica gel desiccant is required. Chemical getters are effective to maintain the pressure below the minimum required for long time by adsorbing residual gases in a VIP core and improve the life span of VIPs. Permeated or out-gassed gases are combined chemically or by adsorption on the surface of getters leading to removal of gases from the evacuated systems. Performance of getters depends upon their sorption capacity. Fumed silica core VIPs do not usually contain getters due to their already longer service life. However, for glass fiber VIPs, getters are usually adopted to increase their short life span. Araki and Kamoto et al. (Araki, Kamoto et al. 2009) used synthetic zeolite getters to adsorb gases for a glass fiber core. Di and Gao et al. (Di, Gao et al. 2014) investigated the use of a novel low cost adsorbent made up of modified calcium oxide (CaO) and copper oxide (CuO) for use in glass fiber core of VIPs and predicted the slower increase in pressure leading to a service life of 10-15 years.

Opacifiers: Opacifiers are used to reduce the radiative conductivity of the core material by making it opaque to infrared radiation. Silicon carbide (SiC) is the most commonly used opacifier in fumed silica core. Other opacifiers such as carbon black, titanium dioxide (TiO_2) and iron oxide (Fe_3O_4) are also being used. Caps and Fricke (Caps and Fricke 2000) reported that at room temperature thermal conductivity of pure silica is higher by 2-3 $mWm^{-1}K^{-1}$ than that of SiC opacified precipitated silica. Nonetheless, caution has to be exercised when using opacifiers as these typically have high solid thermal conductivity which means higher content of opacifier will lead to a higher solid thermal conductivity offsetting any benefit it provides by reducing the radiative conductivity. On the other hand, an insufficient amount of opacifier in a VIP core will lead to a higher radiative conductivity. Hence, an optimum mass proportion of a given opacifier needs to be identified to achieve a minimum radiative conductivity in VIP cores.

Manufacturing of VIPs : Manufacturing of VIPs can be explained briefly as placing core material inside the envelope and heat sealed in evacuated conditions. Core materials are prepared and dried to remove moisture. If necessary, the size of particles is reduced. Then, dried core material is pressed into core boards. Requiring pressure to press core material is varying due to the material. Abe (Abe, Abe et al. 2005) reported that fumed silica and fiber composite boards with sufficient handling strength were obtained by applying 0.6-1.5 MPa pressure. Envelope consists of two or three layers of metalized polymeric films. These metalized polymeric films are heat sealed together in laminate form with proper adhesive. One side of the envelope remains opened for further steps (Alam, Singh et al. 2011). Following to preparation of core board and envelope, core board is putted into the envelope from the open side and placed in the vacuum sealing chamber. Then, chamber is evacuated to the appropriate pressure. So, the open side of the envelope is sealed. Heat sealing of the envelope could be three or four sided. Compared to four sided seal, gas permeation throughout the seal flanges is reduced at three sided seal (Kwon, Jang et al. 2010).

2.3 Heat Transfer Theory in VIPs

Solid conduction, radiation and gaseous conduction are main heat transfer mechanisms in a VIP core. It can be assumed that all these mechanisms occur independently and through the approach of thermal resistance in parallel connection, center of panel thermal conductivity (λ_{cop}) of a VIP can be evaluated as (Fricke, Schwab et al. 2006).

$$\lambda_{cop} = \lambda_S + \lambda_R + \lambda_G + k_C \tag{2.1}$$

where, λ_S is the solid thermal conductivity ($Wm^{-1}K^{-1}$), λ_R is the radiative thermal conductivity ($Wm^{-1}K^{-1}$), λ_G is the gaseous thermal conductivity ($Wm^{-1}K^{-1}$) and k_C is the thermal conductivity due to coupling effect ($Wm^{-1}K^{-1}$). The center of the panel thermal conductivity of a VIP panel is expected to be approximately 4-5 $mWm^{-1}K^{-1}$. By reducing each thermal conductivity term in the right hand side of Equation 2.1, total thermal conductivity of VIP core can be deduced. Coupling effect only become

apparent at high pressures for core materials with large pore size (Fricke, Schwab et al. 2006).

All heat transfer mechanisms that contribute to center of panel thermal conductivity are explained in detail below.

Solid Conduction: In solid conduction mechanism, heat is transferred through the contact of particles. Solid conduction is the most important heat transfer mechanism in core material under vacuum. Thermal conductivity of porous solids is usually much lower than nonporous ones. Also, it depends on material, density, and pressure applied to the core. For powders as core material, heat is transferred through small contact area among particles. Equation 2.2 gives the correlation between solid thermal conductivity and density (Fricke, Schwab et al. 2006).

$$\lambda_s \approx \rho^{\alpha} \tag{2.2}$$

where ρ is density (kgm^{-3}) and the index α has an approximate value of 1 for foams and ranges from 1 to 2 for powders materials depending upon the material structure. Regarding to Equation 2.2, it can be clearly said that the materials with lower bulk density have lower solid thermal conductivity (Fricke, Schwab et al. 2006). Approximately expected solid thermal conductivities are 1-3 $mWm^{-1}K^{-1}$ for fibers, 3-10 $mWm^{-1}K^{-1}$ for powders, and 5 $mWm^{-1}K^{-1}$ for foams (Fricke et al., 2006). Equation 2.2 is not proper for powder materials because of their uneven particle size and random arrangement. Kwon and Jang(Kwon, Jang et al. 2009) reported two models for theoretical calculation of solid thermal conductivity of powder core materials based on Hertz contact theory and assuming cubic or hexagonal arrangement of the powder particles. But, their theoretical calculations for fumed silica were 4 to 12 times higher than its reported value. This huge difference between the theoretical and experimental was thought to be caused by values of the high effective porosity due to uneven and random arrangement of particles. This disagreement is expected to be higher for composite mixtures. Hence, reliable experimental data is required to evaluate exact solid thermal conductivity of powder materials.

Radiation: Radiation is another significant heat transfer mechanism for evacuated core materials. Radiative heat transfer in porous insulation is reduced by

scattering and absorption by adding opacifier to the core material. Radiative thermal conductivities below 1 $mWm^{-1}K^{-1}$ can be achieved with adding suitable opacifier (Bouquerel, Duforestel et al. 2012). Equation 2.3 is an analogous to Fourier law and can be employed to calculate radiative thermal conductivity of a porous core material (Fricke, Schwab et al. 2006).

$$\lambda_R = 16n^2\sigma T_r^3/3E_C(T_r) \tag{2.3}$$

where n is the mean index of refraction, σ is the Stefan-Boltzman constant ($5.67x10^{-8}$ $Wm^{-2}K^{-4}$), E_c is the extinction coefficient of the core material (m^{-1}) and T_r is the average temperature within the insulation material (K). $T_r$is calculated with Equation 2.4,

$$T_r = \sqrt[3]{\frac{1}{4}(T_1^2 + T_2^2)(T_1 + T_2)} \tag{2.4}$$

where T_1 and T_2 are the temperature of VIP surfaces. Extinction coefficient can be calculated by multiplying the specific extinction and density (ρ) of specimen. Specific extinction can be calculated using the measured transmission values which can be obtained by Fourier Transform Infrared spectroscopy (FTIR).

Gaseous thermal conduction: Heat transfer via gas molecules is also possible in porous solids. Gaseous thermal conductivity is related to either internal pressure which is upon to amount of gas in pores or pore size. When the pore size and the mean free path of the gas molecule are equal to each other, all collisions take place between the gas molecule and pore walls. Hence, gaseous thermal conductivity reduces. Equation 2.5 is used to calculate Knudsen number which is the ratio of molecular mean free path (l) to the pore size diameter (Φ) (Simmler and Brunner 2005)

$$K_n = l/\Phi = k_B T/\sqrt{2}\pi d^2 P\Phi \tag{2.5}$$

where k_B is the Boltzman constant ($1.3807x10^{-23}$ JK^{-1}), T is the temperature (K), d is the diameter of the gas molecule (m), P is the gas pressure (Pa). Knudsen number higher than 1 means that mean free path is larger than pore size and all molecules collide elastically with pores and energy is not transferred. At low pressures where Knudsen

number is much higher than 1, gaseous thermal conductivity is low. Higher pressure leads to interaction between gas molecules and increases the gaseous thermal conductivity (Simmler and Brunner 2005). Equation 2.6 gives the relationship between gaseous thermal conductivity (λ_G) and Knudsen number (Kaganer 1969)

$$\lambda_G = \lambda_0/(1 + 2\beta K_n) \quad (2.6)$$

where λ_0 is the thermal conductivity of free gas ($Wm^{-1}K^{-1}$) and β is the gas coefficient. Regarding to Equaitons 2.5 and Equation 2.6, it can be suggested that materials with large pore size need low pressure to decrease gaseous thermal conductivity. Therefore, materials with small pore size, such as nano porous materials, are ideal for VIP applications to minimize thermal conductivity.

Coupling effect: The coupling effect (kc) arises due to a short circuit for the heat flow from one particle to the other through the gas present in the pores. kc is negligible for foams with non-broken structure and can be significant at high gas pressures due to the presence of large number of molecules in voids. However, at low pressure, this term can be negligible. For powder materials such as perlite and diatomite, the values of coupling effect can range between 20 - 30 $mWm^{-1}K^{-1}$ at atmospheric pressure (Fricke, Schwab et al. 2006). This effect cannot be distinctly separated from the other mode of heat transfer and cannot be measured directly. The semi-empirical approximate models were presented for aerogels and expanded perlite, respectively, by Swimm and Reichenaur et al., and Beikircher and Demharter (Swimm, Reichenauer et al. 2009, Beikircher and Demharter 2013). These models are limited to the interaction of gas and solid conduction. Beikircher and Demharter (Beikircher and Demharter 2013) measured the sum of coupling and gaseous conductivity to be 43.9 $mWm^{-1}K^{-1}$ at atmospheric pressure; the coupling effect was estimated to be 0.03 mW $m^{-1}K^{-1}$ for expanded perlite powder at a pressure of 0.08 mbar. The coupling effect at specific pressure can also be calculated by measuring the thermal conductivity of panel both at atmospheric condition and under evacuated conditions provided the gaseous conductivity at atmospheric and vacuum states were known.

CHAPTER 3

EXPERIMENTAL PROCEDURES

3.1 Materials

Calcium hydroxide ($Ca(OH)_2$) was purchased from Merck with a purity of 96% of which 3% was $CaCO_3$, and 1% was other impurities (mainly 0.05% of Na, K, Fe, Sr; 0.5% of Mg; 0.01% of $SO_4^{=}$, and 0.005% of Cl^-). Ultrapure water was obtained with a MilliQ (Millipore- Elix UV5/ Milli-Q) water purification system with a purity of 18.2 μohm at 25 ^oC. Also, deionized water was obtained from a reverse osmosis water purification system with an ion exchange unit. CO_2 gas was purchased from Karbogas, Turkey with a purity of 99.99%.CAB-O-SIL® M-5 fumed silica with a purity of 99.8% was purchased from CABOT, U.S.A. Bulk density of fumed silica was approximately 50 kgm^{-3} and average particle size was about 200-300 nm. BET surface area of particles were about 200 m^2g^{-1}. Polyester fiber (PF) with diameter of 12 μm, length of 6 mm, and melting point of 230-260 ºC was purchased from Petfiber, Uşak, Turkey. Commercial polyamide (PA)/polyethylene (PE) films of 90 and 170 μm were purchased from Vakupak, Izmir, Turkey. Al-PET (Aluminum-Polyethylene terephthalate) was purchased from Hanita Coating, U.S.A.

3.2 Hollow Nano Calcite Production

Hollow nano calcite ($CaCO_3$) production was achieved with the small penetration method initially developed in our laboratory as a result of a project funded by TUBİTAK with a project number of 110M104. The schematic view of the experimental set-up was shown in Figure 3.1. The experimental setup consists of stabilization tank, a reaction chamber, a circulating pump, a stirrer, and measurement probes. 15 mM of $Ca(OH)_2$ solution was prepared in 35 liter of water in the stabilization tank. The solution was stirred with a mechanical stirrer at 1000 rpm to dissolve the $Ca(OH)_2$ and to suspend the produced particles in DI water. The pump operates with a

1.0 m^3h^{-1} of flow rate to take liquid from the stabilization tank and discharge it at the reaction chamber where the dissolved $Ca(OH)_2$ solution returns back to the stabilization tank. In this case, CO_2 was injected into the reaction chamber where CO_2 dissolves on the surface of the freely flowing liquid. The unreacted CO_2 was allowed to leave the reaction chamber from the openings. Crystallization was expected to occur at the surface of the liquid. Because the CO_2 consumed at the surface, it cannot diffuse into the liquid, which is called the small penetration method. Both pH and conductivity were measured in the stabilization tank and continuously recorded by a computer. At certain time intervals, samples were withdrawn from the stabilization tank and analyzed. When the conductivity value was dropped to about zero, the crystallization was terminated by stopping the CO_2 flow. The products obtained were either separated initially by a centrifuge with 50 ml of Falcone tubes, or as developed in this thesis, a fluidized bed filtration system was used to separate the products. Parameters were optimized to produce the desired hollow nano $CaCO_3$ particles.

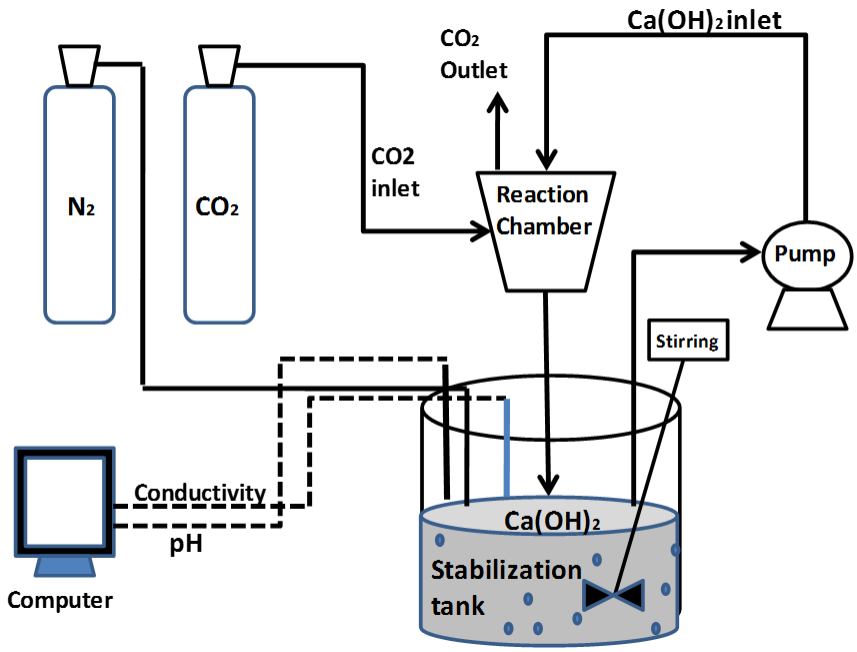

Figure 3.1. Experimental set-up for hollow nano $CaCO_3$ production

3.3 Development of Fluidized Bed Filtration System

A filtration-through ceramic filter was used to separate the hollow nano $CaCO_3$ particles from the liquid suspension. However, in flow-through filtration, the nano particles aggregated on the surface of the filters and annealed each other to form clumps of structures. Therefore, filtration-through was unsuccessful to separate the nano particles. Then, a fluidized bed filtration system was developed to separate hollow nano-$CaCO_3$ particles at large scale. Figure 3.2 shows the schematic of the newly developed fluidized bed filtration system. The system consists of a ceramic filter with a pore size of 900 nm placed within a container jacket. The filter is sealed and integrated to the system as one inlet and two outlets, one of the outlets was for recycled fluid stream and the other was for the discharge filtrate stream. As shown in the figure, the synthesized hollow nano-$CaCO_3$ particles were suspended in a 35 liter stabilization tank. A pump withdrew the liquid suspension from the tank and sends it to the filter where the particles were fluidized in order to keep the particles suspended. In such design, the filtrate was discharged as clear liquid and particulate solution was accumulated in the stabilization tank. Therefore, aggregation and formation of clumpy structures were avoided. It took about 3 hours to filter about 35 liters of suspension. About 1.5 liters of slurry was remained in the tank at the end of filtration, which was centrifuged and dried before its use in VIP panels.

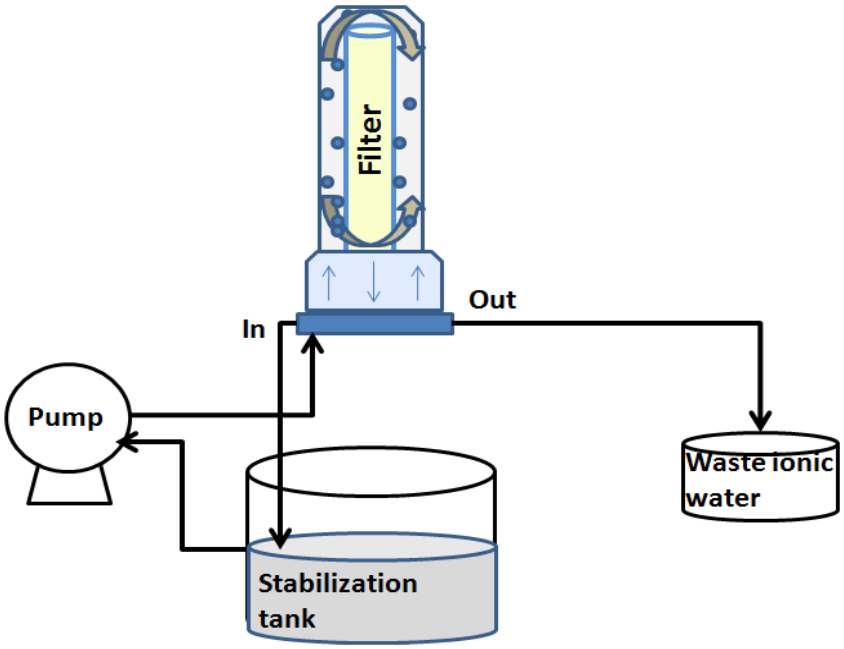

Figure 3.2. The developed fluidized bed filtration system

3.4 Outer Envelope and $ZnSnO_x$ Coating

The polymeric outer envelope was coated with zinc-tin-oxide (ZTO), $ZnSnO_x$, with a high vacuum magnetron sputtering system as shown in Figure 3.3. The system consists of a high vacuum magnetron sputtering section and a roll-to-roll coating design placed within the high vacuum system. The polymeric films were commercial polyamide (PA) / polyethylene (PE) with a thickness of 90 and 170 μm. The thickness of the films was selected with respect to the water transfer rates of the bare films without any coating on it. In order to make ZTO films, 52% Zn and 48% Sn was mixed to form Zn_2Sn (ZT) target in high field magnetic sputtering system. The vacuum pressure was about $2x10^{-5}$ Torr. The effects of O_2 feed rate and wrapping rate on film thickness were investigated. For indium-tin-oxide (ITO) coating, pressure in vacuum magnetron sputtering system was $2x10^{-5}$ Torr. About 2.5 sccm (standard cubic centimeter) of oxygen (O_2) along with argone (Ar), as the carrier gas, were fed to the system. Outer envelope barrier films were produced in different thicknesses by changing the wrapping rates in rpm.

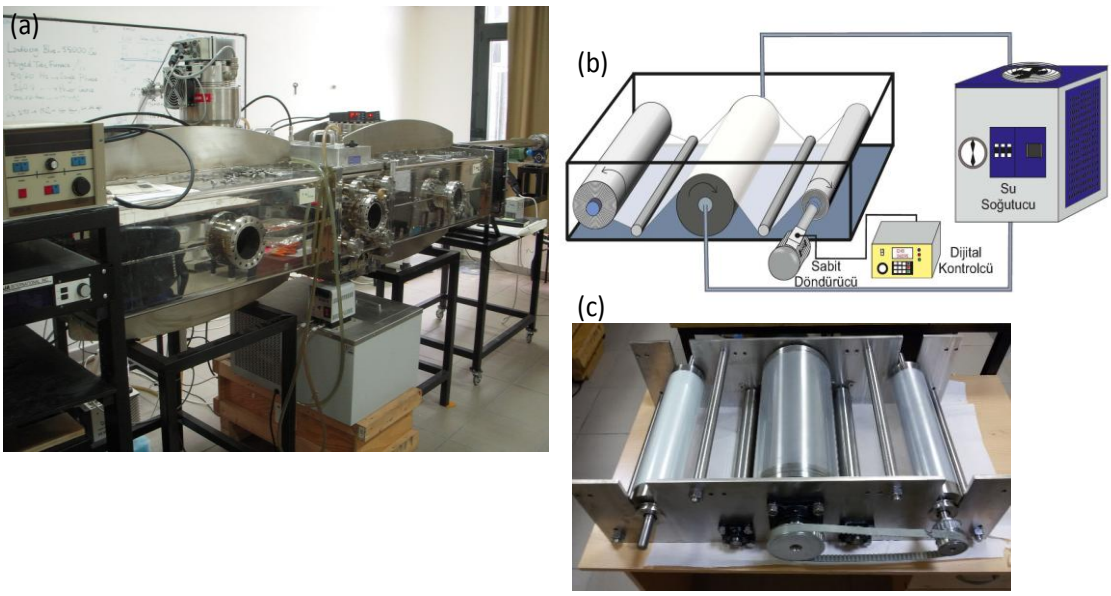

Figure 3.3. (a) Roll to roll high vacuum magnetron sputtering system, (b) roll-to-roll coating design, (c) actual manufactured roll-to-roll film coating settings

3.5 Vacuum Insulation Panel (VIP) Production

Figure 3.4 shows the pictures and processes for the production of vacuum insulating panels. VIPs consisted of three materials for thermal resistance such as a core material, a dust tight inner envelope (textile bag), and an outer envelope. The core material consisted of the filling core and a binding material. Figure 3.4a shows fumed silica as the commonly used core material in VIPs. The binder used was a polyester which was aligned on a winding machine and cut into pieces to reduce its lengths to about 6 mm (Figure 3.4c-d). Hollow nano-calcite was developed as an alternative core material for this study (Figure 3.4b). The core material and the binder were mixed in the mixing container (Figure 3.4e-f). According to panel size and material ratios, proper amounts of materials were weighted and mixed for 2 hours in mixer. Mixed core material was putted into a mold (Figure 3.4g) and compressed with pressures up to 60 bar for 90 seconds (Figure 3.4j). Then, the molded core material was covered with a 20 gm^{-2} of commercial textile bag with an inner envelope or primary cover material in order to keep the core material as a whole (Figure 3.4l). Without delay, core material was coated with outer envelope. While the inner envelope was purchased, the outer envelope was prepared in this study. Commercial Al-PET was also used as the outer cover material. The outer cover of polymeric films was sealed (Figure 3.4m) and the prepared VIPs inserted into the vacuum packing system. VIPs were vacuumed by the vacuum packing machine (LIPOVAK) (Figure 3.4n).Vacuum was applied up to 1 mbar or 10^{-5} Torr. Different types of VIPs were produced and tested for characterizations (Figure 3.4o).

The panel size was chosen as 27 x 27 x 2 cm^3. For fumed silica panels, the percentage of polyester binder as the filling material was 16.5wt %. Other core materials studied in this thesis included 10wt% of polyester binder due to its heavier weight. In a separate study, the commercial fumed silica and hollow nano calcite were used as the core material at various ratios as summarized in Table 3.1.

Figure 3.4. Pictures and processes for the production of vacuum insulating panels (a) Fumed silica as core material, (b) hollow nano calcite developed for this study, (c) winding the polyster binder for cut, (d) polyester cuts, (e) mixing of core and binder materials, (f) mixer container, (g) moulding machine with press, (h) filling the core material in the moulding, (i-j) compressed core material for VIP, (k) moulded core material ready for VIP making, (l) inner envelope or primary cover material, (m) commercial Alumina-PET, (n) vacuum packing system, (o) product of different types of VIPs.

Table 3.1. Hollow nano calcite, fumed silica and polyester fiber mixing ratios for the core material preparation

Material	Hollow Nano Calcite (%)	Fumed Silica (%)	Polyester Fiber(%)
#1 VIP	0	90	10
#2 VIP	3	87	10
#3 VIP	10	80	10
#4 VIP	45	45	10
#5 VIP	90	0	10

3.6 Characterizations

Average particle size and size distribution for hollow nano $CaCO_3$ were measured using dynamic light scattering (DLS) method. About 1 mL of sample was withdrawn from the solution into a UV cuvette and size and size distribution were measured using particle size analyzer (Malvern nano sizer, ZS model). At certain time interval, precipitates were separated from sampled solutions by centrifugation (Universal 320 – Hettich Zentrifugen) at 9000 rpm for 20 min. The particles were washed with acetone and dried at 103 ^{o}C in an oven (Nüve FN 500) overnight. The morphologies of the $CaCO_3$ crystals were analyzed using a scanning electron microscope (SEM) equipped with a field emission source (Philips XL 30 S FEG), operating at an accelerating voltage of 15 kV.

Water vapor transmission rate (WVTR) of each film was obtained by the ASTM E96 method as shown in Figure 3.5. Briefly, a pre-weighted amount of water containers was sealed with the indicated polymeric films and their weights were measured over time. Any decrease in weight over time is related to the water vapor transfer rate from the films according to Eq.3.1.

$$WVTR = \frac{m * 24}{A}, \quad \left(\frac{g}{m^2.day}\right) \tag{3.1}$$

Here, *m* is the slope for water weight loss in g/hr, *A* is the area of the film in m^2. The water transfer rate values were compared with the commercial Al-PET (Aluminum-Polyethylene terephthalate) film.

Figure 3.5. Water vapor transmission rate (WVTR) measurement system

Thermal conductivity of VIP was measured by a guarded plate apparatus as shown in Figure 3.6. The apparatus was designed for sample panels of sizes 27 × 27 × 2 cm for low thermal conductivity values. Before measurements, the equipment was first calibrated using conventional glass wool. Then, the thermal conductivities of VIPs were measured over a measuring zone 25 mm × 25 mm. The accuracy of the device was about ±2 $mWm^{-1}K^{-1}$. The mean temperatures of the samples were adjusted to about room temperature of 22 ± 1 ºC so that the cold side was adjusted to 14 ± 1 ºC and the warm upper side was held at 30 ± 1ºC by the apparatus. Thermal conductivity was calculated from Fourier`s law using the temperatures at both sides of the plates, the heat input, and thickness of the samples. Thermal conductivity of VIPs produced using different core materials were measured at different vacuum pressures.

Figure 3.6. Thermal conductivity measurement equipment, (a) pump system, (b) thermal conductivity measurement device (Linseis HFM 300), (c) pressure indicator panel, (d) pressure gage.

CHAPTER 4

RESULTS AND DISCUSSION

4.1 Production of Hollow Nano Calcite Particles

Hollow nano-calcite particles were produced using the small penetration method which was developed by the TUBITAK funded project in our lab.$Ca(OH)_2$ solution of 15 mM was prepared within 35 liter of deionized water. The pump was operated to circulate the liquid solution between the stabilization tank and reaction chamber. CO_2 was injected into the crystallization chamber where it diffuses into the solution and nano-$CaCO_3$ particles were formed. The changes in pH and conductivity values were monitored to follow the reaction conditions as shown in Figure 4.1. As shown in the figure, conductivity decreased almost linearly as calcium (Ca^{++}) ions were consumed to produce $CaCO_3$ particles while decrease in pH was slight. When all Ca^{++} ions were consumed, conductivity almost reached to zero and then a sudden decrease in pH occurred. At the completion of the $CaCO_3$ synthesis, the reaction was terminated by stopping the CO_2 flow.

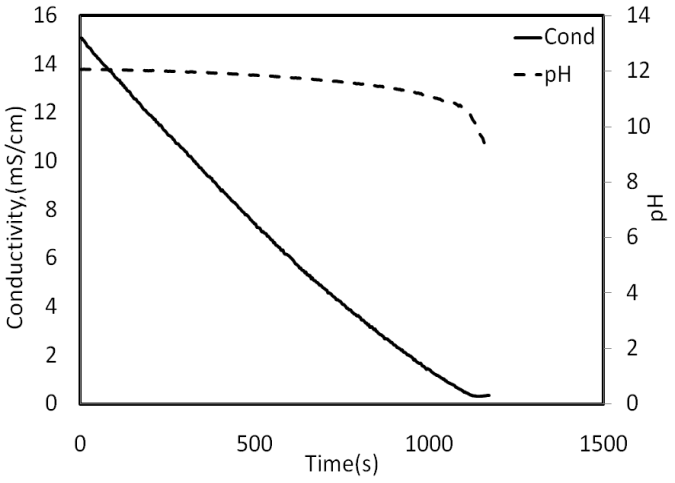

Figure 4.1. pH and conductivity values during $CaCO_3$ crystallization

Figure 4.2 shows the SEM images of the hollow nano $CaCO_3$ particles produced using the small penetration method. As can be seen in the figure, the produced particles are about 300 nm in size and their pores are about 40 nm. It was also seen that these particles are almost in homogenous size distribution. The production method was satisfactory to produce the desired hollow nano-$CaCO_3$ particles. However, separation of these particles from the liquid suspension was a challenge.

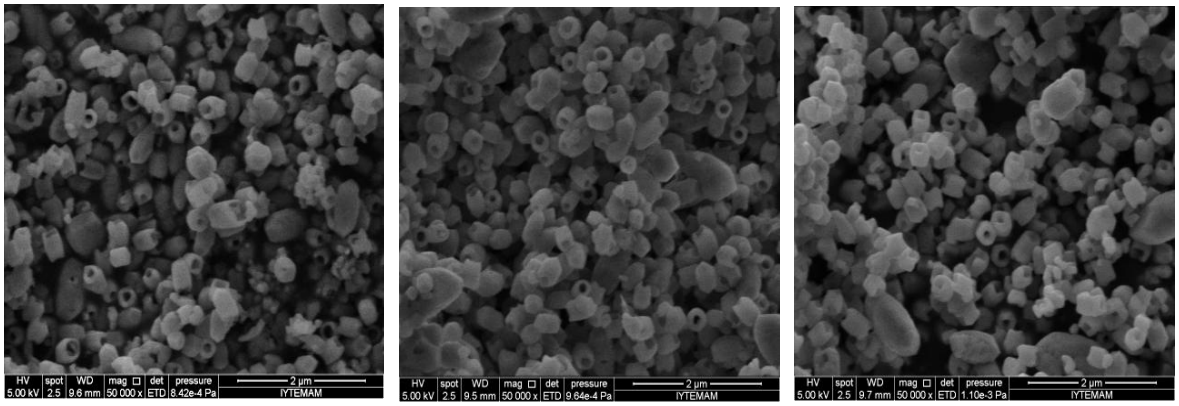

Figure 4.2. Hollow nano $CaCO_3$ particles produced using the small penetration method

Initially, the produced hollow nano-$CaCO_3$ particles were separated by centrifugation. In this method, liquid suspension was placed in a 50 mL Falcone tubes and centrifuged at 9000 rpm for about 7 minutes. Six Falcone tubes, a total of 300 ml of fluid suspension, were used at each centrifugation. Therefore, centrifugation method took time and was not practical to produce large quantity of particles.

Then, a ceramic filter was used to separate nano particles from the liquid slurry. In this method, a ceramic filter with a pore size of 900 nm was placed in a plastic holder and secured against leakages. A flow-through filtration was applied to separate the liquid from the suspended nano particles. Although the porosity of the ceramic filter was reported to be 900 nm, no particles were detected at the filtrate stream due to large thickness of the filter. It was thought that the nano particles were accumulated on the surface and within the porosity of the filter and decreased the area to the flow so that a nice cut-off was achieved to separate 300 nm of hollow nano $CaCO_3$ particles. Figure 4.3 shows the products obtained from the flow-through filtration. As can be seen from the figure, particles were adsorbed on the surface of the filter during the filtration and highly aggregated. The figure also shows that these particles were stuck on the surface and dissolved by fluid flowing during the filtration. The dissolved ions in turn deposited

on the other particles resulting in close up of hollow openings on the particles with a recrystallization. Therefore, highly aggregated particles with clumpy of structures were obtained. Also, an increase in temperature was seen from 25^{o}C to 40^{o}C during filtration. Higher temperatures could lead to the enhancement in dissolution and aggregation of particles in the filtration system. As a result, a flow-through filtration process was unsuccessful.

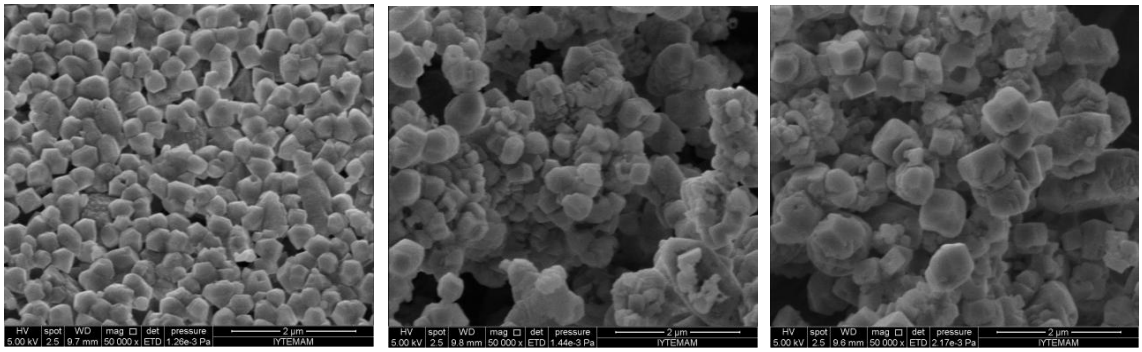

Figure 4.3. Product obtained from flow-through filtration

In order to solve the dissolution-recrystallization and the aggregation problem, a fluidized bed filtration system was designed as shown in Figure 3.2. Hollow nano-$CaCO_3$ particles were synthesized in a 35 liter of 15 mM of $Ca(OH)_2$ solution by the small penetration method. The hollow nano-$CaCO_3$ particles were synthesized when the conductivity values were close to the zero as indicated in numbers on Figure 4.4. As shown in the figure, conductivity decreases almost linearly as the crystallization progress. Conductivity at point 2 indicates that the Ca^{++} ions almost completely consumed in the solution. After the zero conductivity, the conductivity values were seen to increase due to the increase in other ions form the dissolution of CO_2 such as $CO_3^{=}$, HCO_3^{-}, $CaHCO_3^{+}$ and from the dissolution of the newly produced $CaCO_3$ particles such as Ca^{++}, $CO_3^{=}$, and $CaOH^{+}$ ions. Samples were taken from the indicated time intervals; solid particles were separated by centrifugation, dried in an oven at 110 ˚C, and their SEM images were taken.

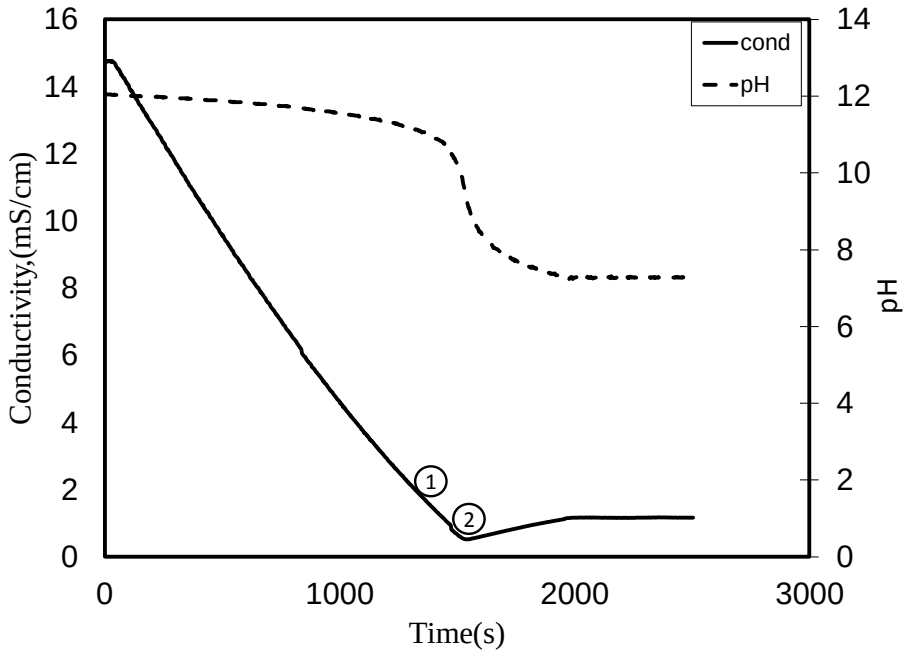

Figure 4.4. pH and conductivity values for the synthesis of hollow nano$CaCO_3$ particles by small penetration method. Numbers indicates the samples taken during the experiment.

Figure 4.5 shows the SEM images of the particles synthesized at the indicated time intervals during $CaCO_3$ crystallization. The formation of hollow nano-$CaCO_3$ particles has been studied extensively in our group and was not thoroughly discussed in this thesis. Briefly, as shown in the figure, at the conductivity value of 2500 $mScm^{-1}$, particles were in rice-like shape and the pores did not form. When these rice-like particles pass through the CO_2 diffusion environment in the reaction chamber, these particles started to dissolve from their end sides forming pores within the particles. At about zero conductivity, almost all Ca^{++} ions were consumed and a driving force appeared to dissolve the nano $CaCO_3$ particles in Ca^{++} deficient solution. As a result, a porosity was developed within the nano-$CaCO_3$ particles. As shown in the figure, hollow nano-$CaCO_3$ particles were produced at conductivity at about 750 $mScm^{-1}$.

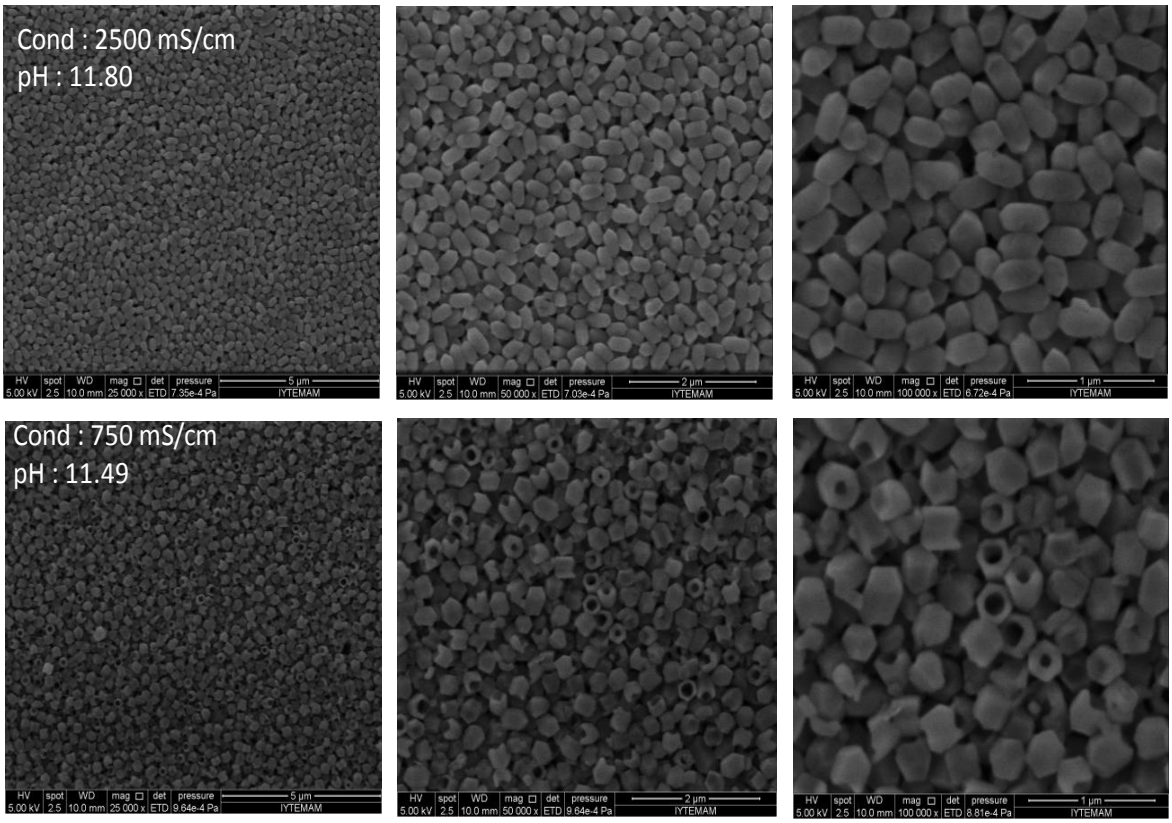

Figure 4.5. SEM images of rice-like and hollow nano $CaCO_3$ particles

The developed fluidized bed filtration system was used to separate the hollow nano-$CaCO_3$ particles. Figure 4.6 shows sample taken during the filtration in the developed fluidized bed filtration system and final filtered product. As shown in the figure, particles synthesized were hollow nano-$CaCO_3$ particles with almost homogenous size distribution. The fluidized condition did not smash the particles on the surface of the filter, otherwise, it would cause the dissolution and aggregation of particles. At the end, hollow nano-$CaCO_3$ particles could be obtained in the developed fluidized bed filtration system.

The developed novel separation approach has some advantages such as reduced centrifugation volume, short process times, and increase in final product volume due to avoiding agglomeration and cementing.

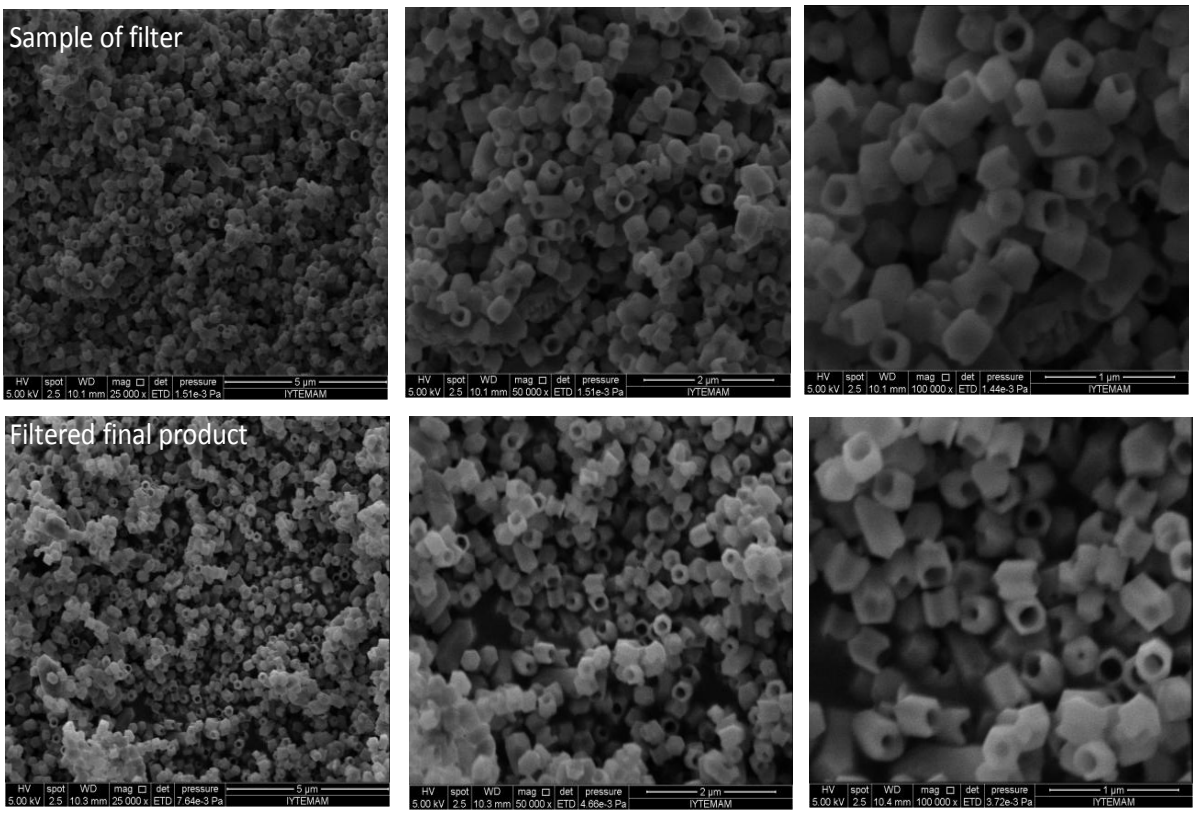

Figure 4.6. Sample taken during the filtration in the developed fluidized bed filtration system and final filtered product

The filtrate was discharged from the fluidized bed filter with free of particles. Because an extensive amount of water is used in crystallization, it was proposed to reuse the waste water from the filtrate. Therefore, in a separate experiment, the water from the filtrate was recycled to use in the crystallization. Figure 4.7 shows the $CaCO_3$ particles synthesized in the presence of waste water from the filtrate from the fluidized bed filtration system. As can be seen from the figure, the particles produced from the effluent of the filtration system were highly aggregated and formed a clumpy structure. There was no hollow porosity in these particles. It was thought that the ions discharged from the filtration system highly affected the particle formation in the crystallization system.

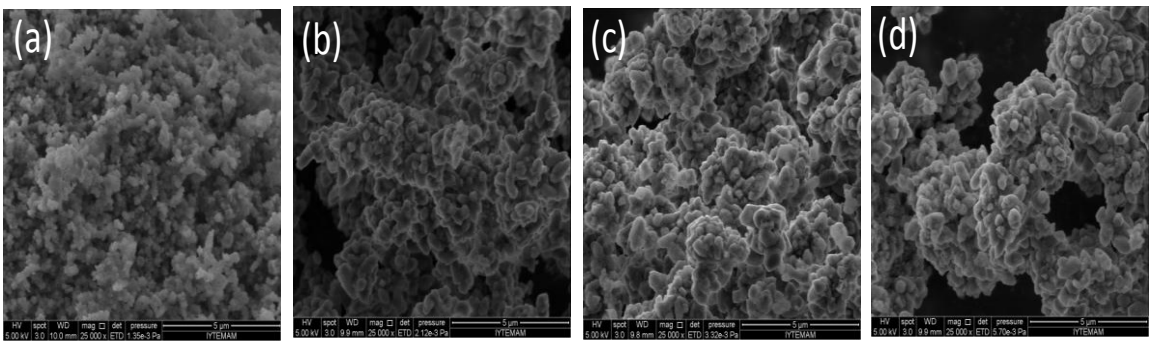

Figure 4.7. Effect of waste water from the filtrate of the fluidized bed filtration system on the $CaCO_3$ particles synthesized

An industrial water purifying equipment operating with reverse osmosis and ion-exchange resin was established in our laboratory to produce hollow nano $CaCO_3$ particles. The small penetration method was used to produce nano $CaCO_3$ particles using the deionized water taken from the reverse osmosis system before the ion exchange. It was seen that an extensive number of air bubbles were developed in the stabilization tank due to the dissolution of air at high pressures in the water tank. As can be seen in Figure 4.8, the particles obtained in such condition were not pleasant. As can been in the figure, the presence of air bubbles in the stabilization tank resulted in aggregation of particles and hollow nano-$CaCO_3$ particles could not be produced.

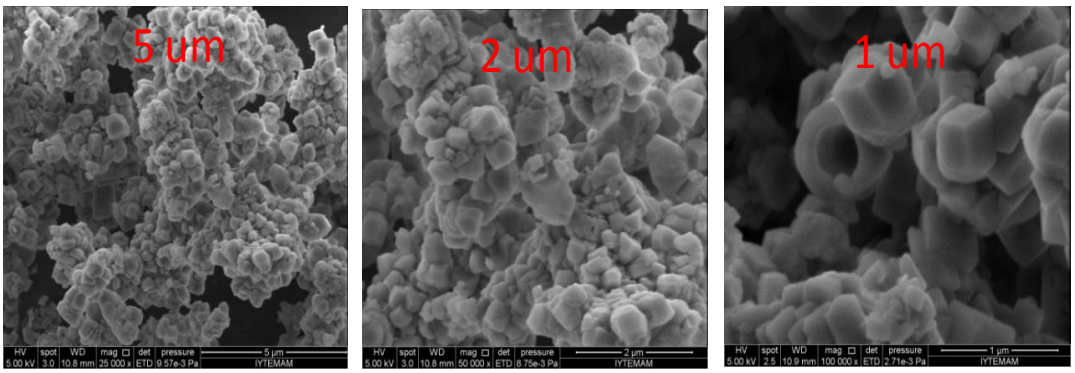

Figure 4.8. SEM images of the calcite particles produced in the presence of air bubbles in the stabilized tank

Nitrogen (N_2) gas was used to remove the air bubbles from the stabilization tank before starting the crystallization experiment. Figure 4.9 shows the SEM images of the particles obtained from the water after removing the air bubbles by N_2. As shown in the figures, well-defined hollow nano-$CaCO_3$ particles could be produced with 300 nm of

particle size with about 40 nm of pore size and homogenous particle size distribution. It was concluded that the water quality is very important in hollow nano $CaCO_3$ particle synthesis.

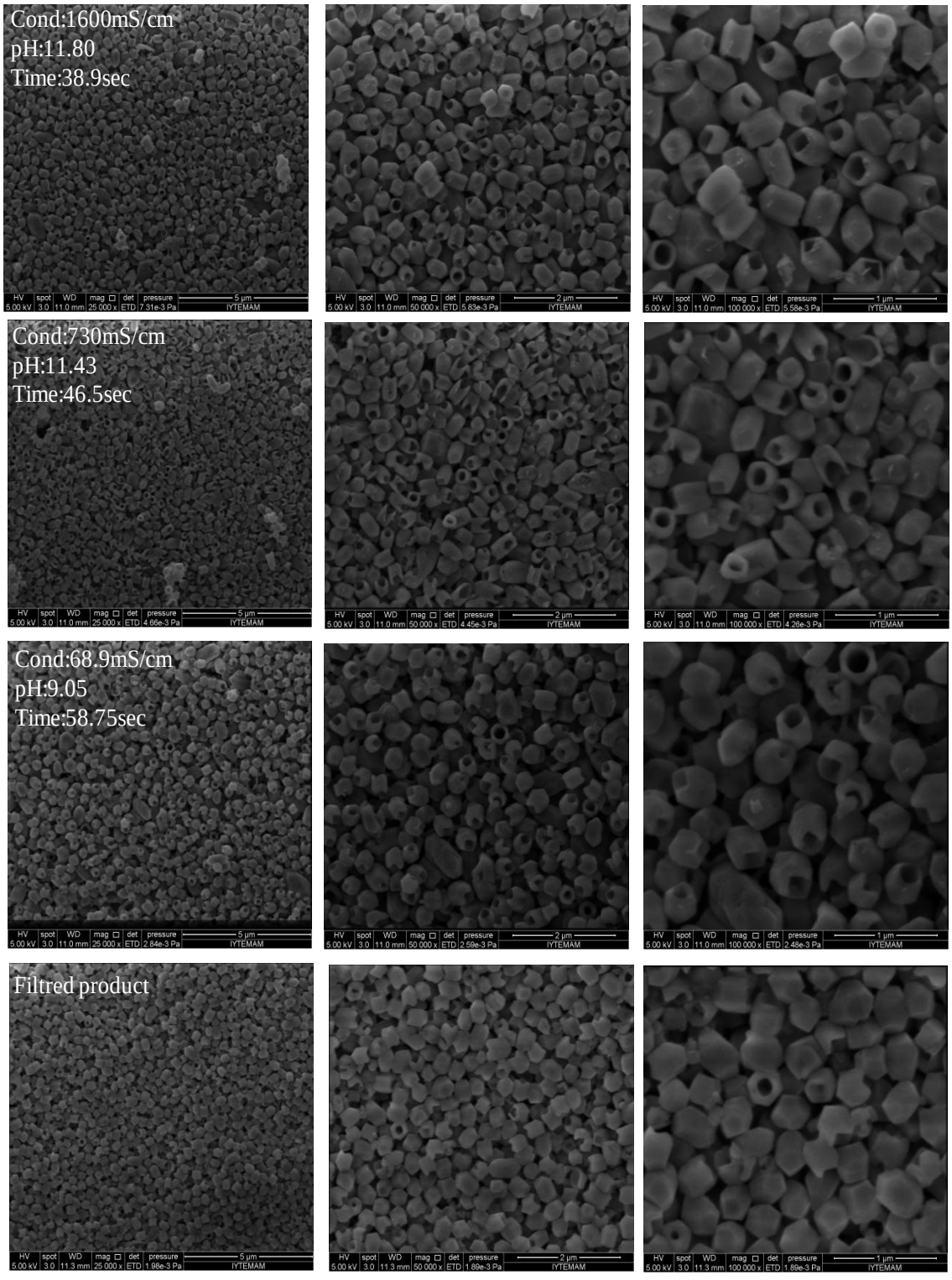

Figure 4.9. Production of hollow nano $CaCO_3$ particles after removing air bubbles from the water in the stabilization tank

4.2 Barrier Material Coating and Characterization

Water vapor transfer rates (WVTR) are important for the stability of vacuum insulation panels. The barrier coating films are one of the components for lower WVTR measurements. We have tested two bare polyamide (PA)/polyethylene (PE) films at two different thicknesses, one is at 90µm and the other is at 170 µm. Figure 4.10 shows the measurement results for WVTRs through the bare PA/PE polymeric films. As can be seen from the figure, the WVTR was calculated as 6.62 $gm^{-2}day^{-1}$ for 90 µm of PA/PE films and 12.06 $gm^{-2}day^{-1}$ for 170 µm of PA/PE films. Comparing to the measured WVTR of 8.819 $gm^{-2}day^{-1}$ for the Al-PET film of about 350 µm thickness, we have decided to use the 90 µm of PA/PE films for coating applications.

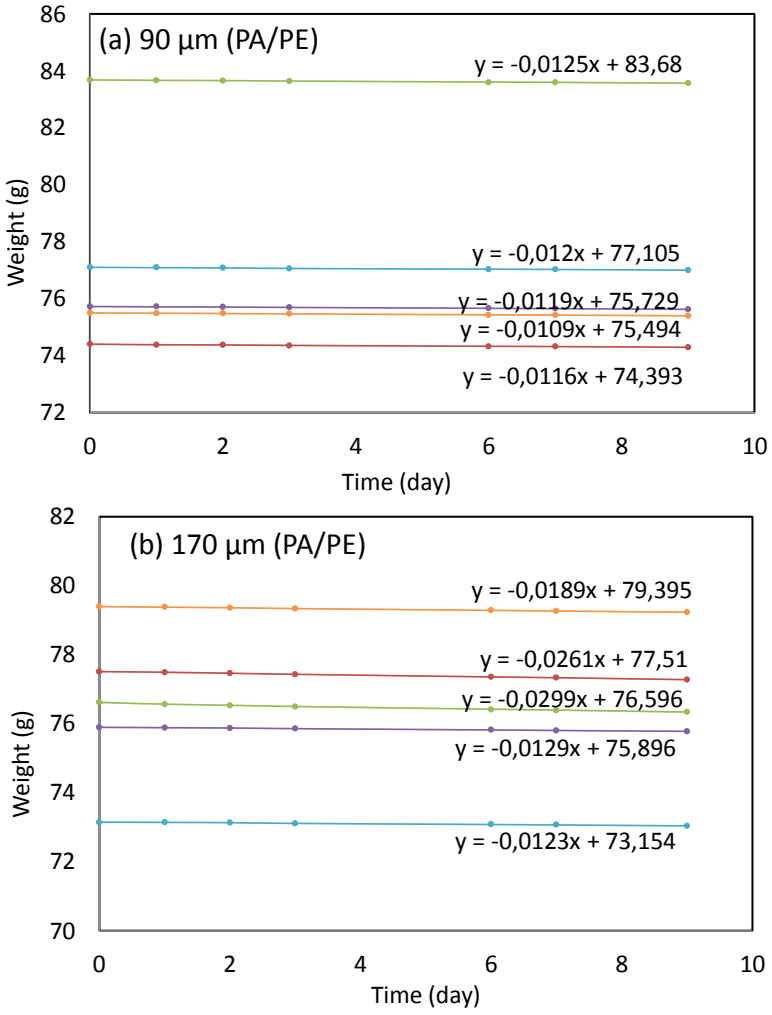

Figure 4.10. Water vapor transfer rate (WVTR) measurement results for (a) 90 µm and (b) 170 µm of bare polyamide (PA)/polyethylene (PE) films

For the following studies, 90 μm of PA/PE films were coated with indium-tin-oxide (ITO) and zinc-tin-oxide (ZTO). For this purpose, firstly PA/PE films were wrapped on the roll system as shown in Figure 3.3, and then, this roll system was placed into the high field magnetic sputtering system. The system was set under high vacuum of about 10^{-5} Torr. O_2 and Ar, as the carrier gas, were fed to the system at indicated rates. The roll wrapping speed was adjusted to the desired level. The anode was the polymeric film and the cathode was the sputtering metal plate, which was set to certain magnetic field. The metals removed from the cathode surface was oxidized in the high vacuum and deposited on the polymeric surface at the anode. Therefore, different thicknesses of the coatings were achieved according to the O_2 content and wrapping speed. Figure 4.11 shows ITO and ZTO coated films in different wrapped rates and feed conditions.

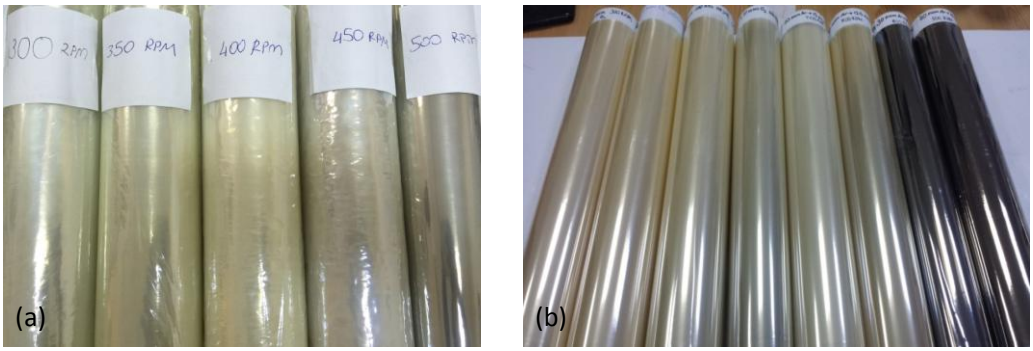

Figure 4.11. (a) ITO and (b) ZTO coated films in different wrapped rate and feed conditions

Effect of wrapping rate on water vapor transmission rate (WVTR) was examined for ITO coatings. Polymeric films of 90 μm in thickness was coated with ITO under high vacuum of $2x10^{-5}$ Torr and 40 sccm Ar (g)+2.5 sccm O_2 (g) flows. The roll to roll rpm rates were adjusted so that the velocity of surface coating varied. Thus, coatings of different thicknesses were obtained. Three samples were tested for each moisture permeability measurements. The results were given in Figure 4.12. As shown in the figure, the WVTR increases slightly with increasing the roll speed. This result indicated that the ITO film thickness became smaller when the rpm of the roller was increased, which caused higher water vapor transmission.

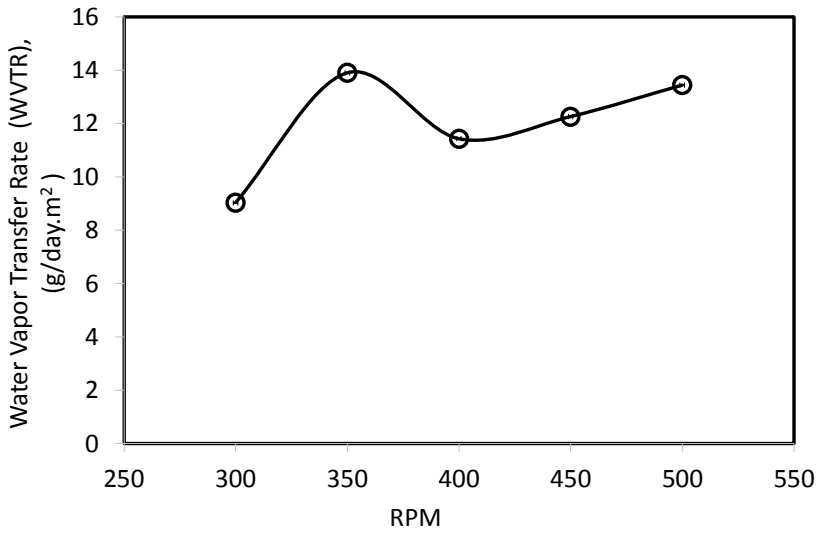

Figure 4.12. Water vapor transfer rate (WVTR) measurement results for 90 μm PA/PE coated with indium tin oxide (ITO)

Coating the polymeric PA/PE films with zinc-tin-oxide ($ZnSnO_x$), or ZTO, were investigated at different roll speed while the O_2 feed percent was constant, and at different O_2 feed percent while the roll speed was fixed. Figure 4.13a shows the water vapor transfer rate. Error bars show the deviations from at least 3 to 5 measurements. As shown in the figure, when the roll speed increased, the water vapor transfer rate for the ZTO coating showed a decreasing trend. It seems that the thickness of the ZTO film decreased with the increased roll speed, however, the surface of the PA/PE film would be more homogenously coated, yielding a less WVTR. It is therefore concluded that the best barrier properties were obtained by the highest wrapping rate. Therefore, the films coated with 30 sccm of constant Ar flow and 7.5, 10, 12.5 and 15 sccm of O_2 feed at 500 rpm roll speed were produced. Figure 4.13b shows the water vapor transfer rate with the O_2 flow percent at fixed roll speed. As shown in the figure, the WVTR slightly increases with the O_2 flow percent. It seems that higher O_2 flow percent increases the amount of metal oxides. We presume that the increase in the oxidized form of ZTO increases the thickness of the metal oxide on the polymeric film which accelerate the transportation of the water vapor. The best WVTR values were obtained at 7.5 sccm of O_2 feed rate. It was concluded that using less O_2 percent in the gas stream would be more advantageous.

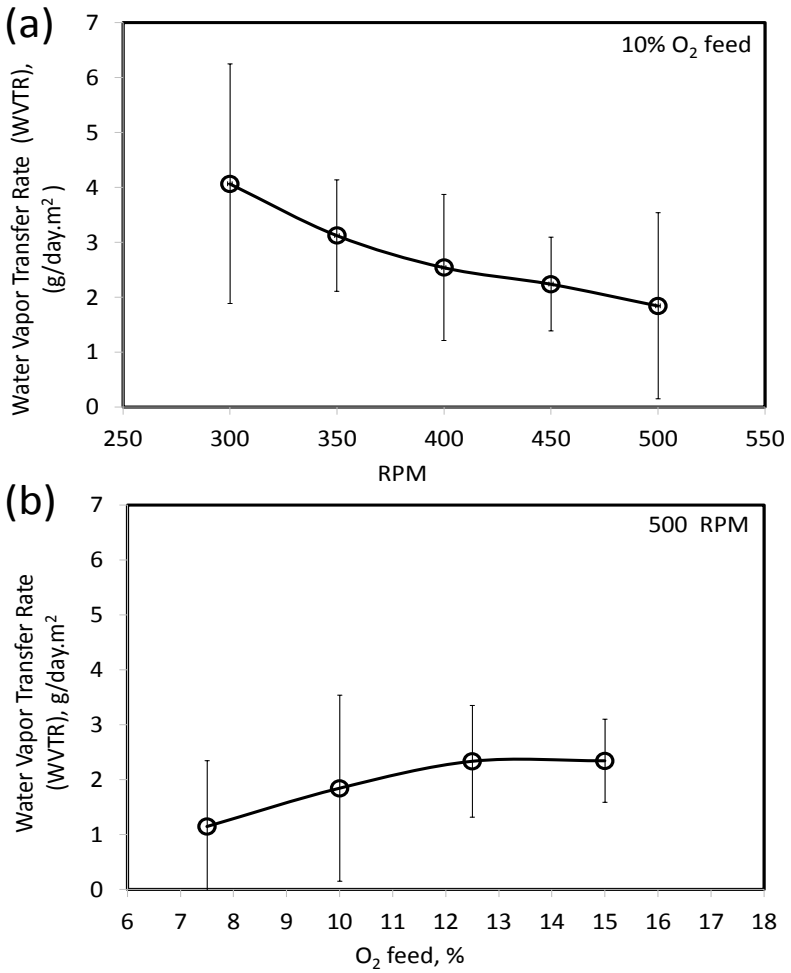

Figure 4.13. Effect of (a) roll speed and (b) O_2 feed percent on water vapor transfer rate.

Figure 4.14 compares the water vapor transmission results for ZTO coatings obtained at different roll speeds at different O_2 feed percentages. As shown in the figure, the WVTR decreases with increasing roll speed for each O_2 percent. It is also shown that the WVTR is much lower at lower O_2 contents. Thus, it is concluded that a better insulation can be achieved by increasing the wrapping rates for the ZTO coating at lower O_2 contents.

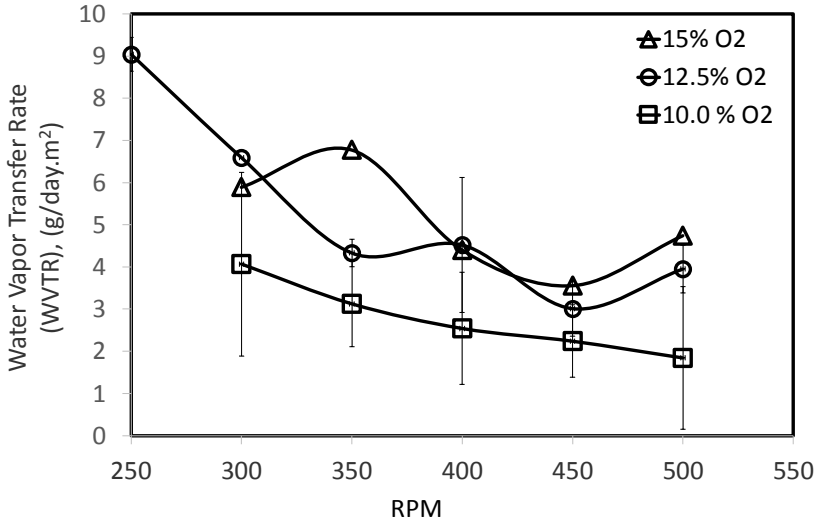

Figure 4.14. Comparison of water vapor transmission test results for ZTO coating for different roll speed at different O_2 feed percent

Polyethylene Terephthalate (PET) polymeric films were also tested for water vapor transfer rates. PET films of 25 μm were coated by ZTO at different wrapping rates in 30 sccm of Ar and 7.5 sccm of O_2 feed and vapor transmission rates were measured. Figure 4.15 shows the WVTR from the ZTO coated PET films of 25 μm. As shown in the figure, contrary to the PA/PE films, the vapor transmission rate increases with increasing wrapping speed for the PET films. Compared to the PA/PE films of 90 μm, the ZTO coated PET films showed worse barrier properties. It was concluded that the PA/PE films have better outer envelope than PET films for the VIP production.

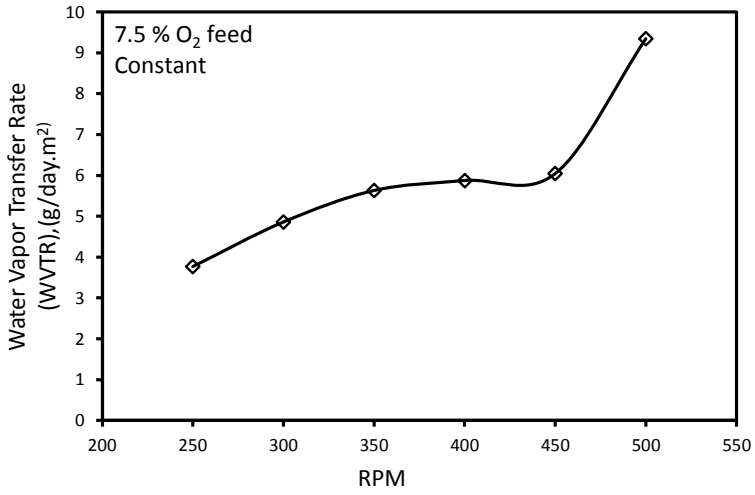

Figure 4.15. WVTR from the ZTO coated PET films.

4.3 Vacuum Insulation Panel (VIP) Production and Characterization

Fumed silica is widely used core material in vacuum insulation panels. In this thesis, a new core material was tested as a candidate, hollow-nano-$CaCO_3$ particles, which is one of our in-house products. Figure 4.16 shows images of vacuum insulation panels (VIP) with 90 μm of PE/PA outer envelope and core materials using fumed silica and hollow nano calcite for comparisons. The panel dimensions were 27x27x2 cm^3 for the VIPs. The prepared VIPs were vacuumed to approximately 10^{-5} Torr in the vacuum system. The further vacuuming was not possible due to the leakages occurred from the sealing in the vacuum system and in the seals on polymeric covers.

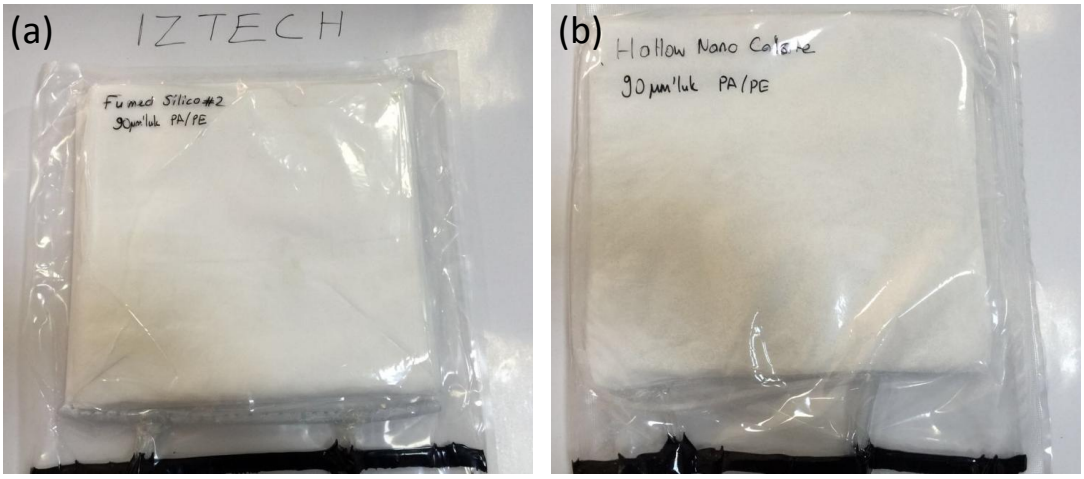

Figure 4.16. Images of vacuum insulation panel (VIP) with 90 μm of PE/PA outer envelope and core materials with (a) fumed silica and (b) hollow nano calcite

In the VIPs, hollow nano calcite particles were mixed with the polyester fibers with diameter of 12 μm, length of 6 mm, and melting point of 230-260 ºC. These fibers were extremely strong, durable, resistant to most chemicals, resistant to stretching and shrinking. Polyester fibers burns slowly and melts at high temperatures. Polyester is hydrophobic in nature and dries quickly which is an advantage for rapid drying of the VIP cores. Therefore, the polyester fibers were obtained commercially and mixed with fumed silica and hollow nano calcite particles to increase mechanical strength of the core board. Figure 4.17 shows the SEM images of polyester fibers and hollow nano

calcite particles as the VIP core material. As can be seen in the images, about 250 nm of hollow nano calcite particles attached to the surfaces of the polyester fibers having a diameter of 12 μm and a length of 6 mm. About 40 nm of pore space in the hollow nano calcite particles can also be shown clearly in the images.

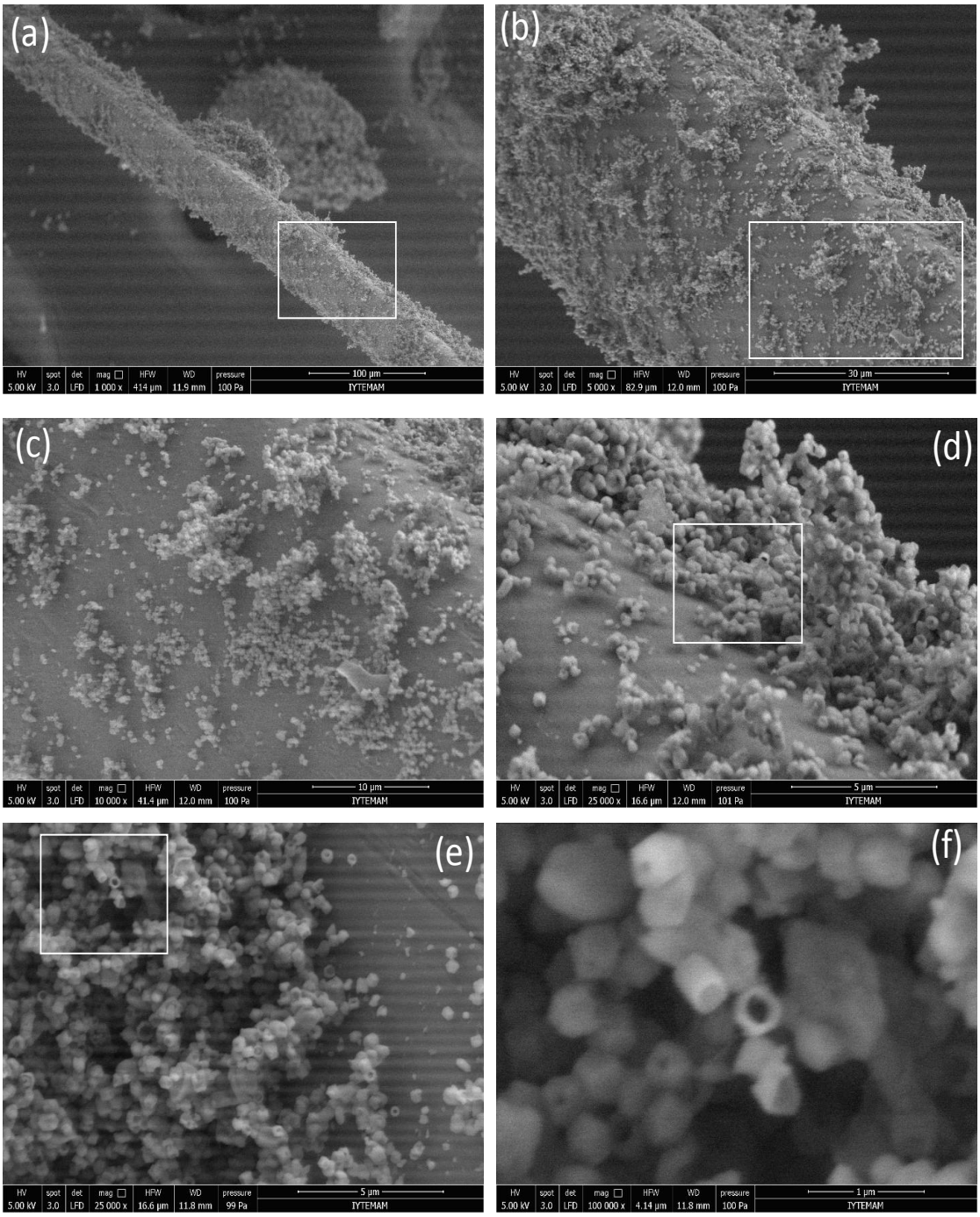

Figure 4.17. SEM images of hollow nano calcite particles mixed with polyester binder fibers for VIP core material.

The thermal conductivity values of the VIPs were measured for fumed silica and hollow nano calcite to be about 28 $mWm^{-1}K^{-1}$ and 64 $mWm^{-1}K^{-1}$ at ambient pressure, respectively. As shown in Figure 4.18, the measured thermal conductivity decreased when vacuum pressure was decreased. The thermal conductivity for fumed silica was about 9.9 $mWm^{-1}K^{-1}$ at about 3.5 Torr while the thermal conductivity for hollow nano calcite particles was about 46 $mWm^{-1}K^{-1}$ at 1.8 Torr. The thermal conductivity of hollow nano calcite was relatively higher than those for the fumed silica. Comparing the packing density of fumed silica and hollow nano calcite, the packing density of fumed silica was about 175 kgm^{-3} and that for the nano calcite was about 667 kgm^{-3}.The fumed silica is much lighter than the hollow nano calcite, or the hollow nano calcite is almost 4 times denser than that of fumed silica. Considering about 2740 kgm^{-3} of the bulk density of the $CaCO_3$, the reduction of packing density of hollow calcite to 667 kgm^{-3} was a success. However, it did not compete well with a better thermal conductivity of the fumed silica.

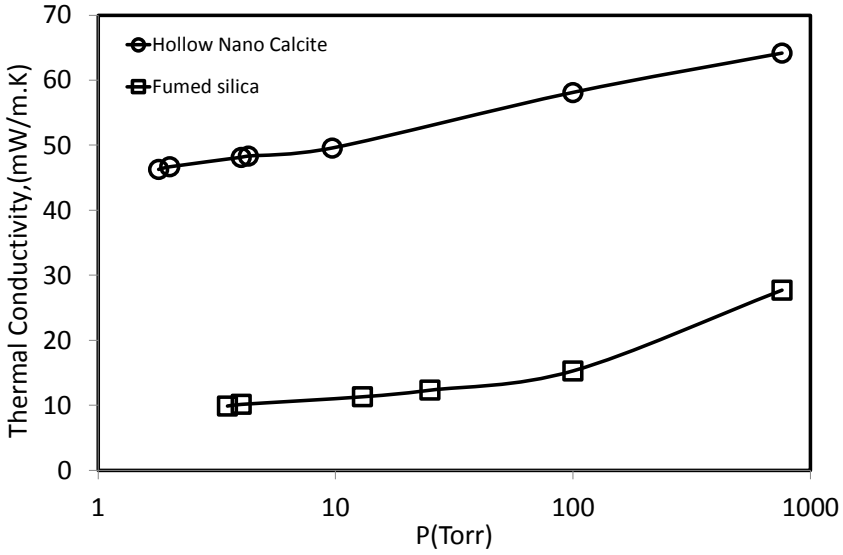

Figure 4.18. Thermal conductivities of VIPs filled with fumed silica and hollow nano calcite as the core materials

Mixing hollow nano calcite particles with fumed silica may improve the thermal conductivity of the VIPs. For this purpose, hollow nano calcite and fumed silica were mixed at different ratios and their VIPs were prepared. Figure 4.19 shows VIPs prepared from fumed silica, hollow nano calcite, and different mixtures of 3 wt% hollow calcite in fumed silica, 10 wt% hollow calcite in fumed silica, and 45 wt%

hollow calcite in fumed silica. The polymeric cover films were uncoated 90 μm of PA/PE for fumed silica and hollow nano calcite. $ZnSnO_x$ coated 90 μm of PA/PE polymeric cover films were used for the core material composed of fumed silica and hollow nano calcite at different ratios.

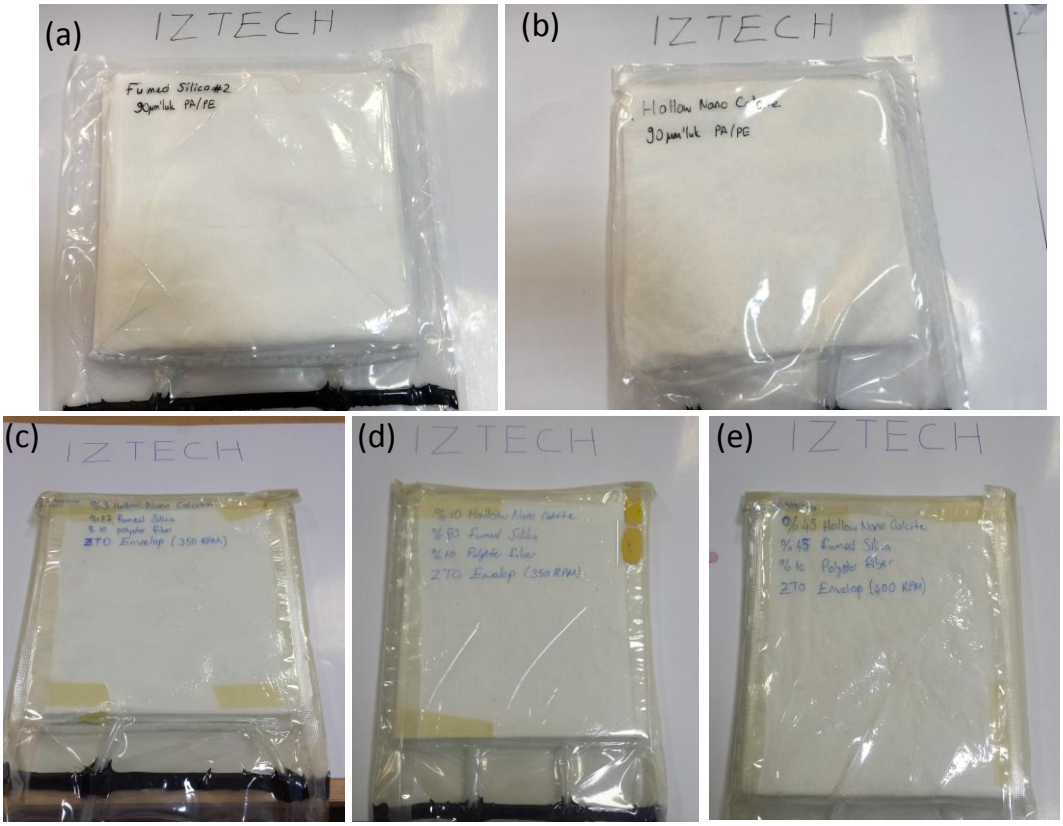

Figure 4.19. VIPs prepared from (a) fumed silica, (b) hollow nano calcite, (c) 3 wt% hollow calcite in fumed silica, (d) 10 wt% hollow calcitein fumed silica, and (e) 45 wt% hollow calcitein fumed silica

Figure 4.20 shows the SEM images of hollow nano calcite particles mixed with fumed silica to form core material for the VIPs. As can be seen from the figure, the fumed silica particles are much smaller than the hollow nano calcite particles. The size of the fumed silica particles is about 10 nm and aggregated to form fumed silica flocks. The calcite particles, on the other hand, is about 300 nm and much bigger than the fumed silica particles. Therefore, the mechanical strength of the VIP is weaker for the fumed silica particles compared to the hollow nano calcite particles as the core material. It was expected that mixing of the fumed silica with the hollow nano calcite particles

would improve the mechanical strength and the thermal conductivity of the composite VIPs.

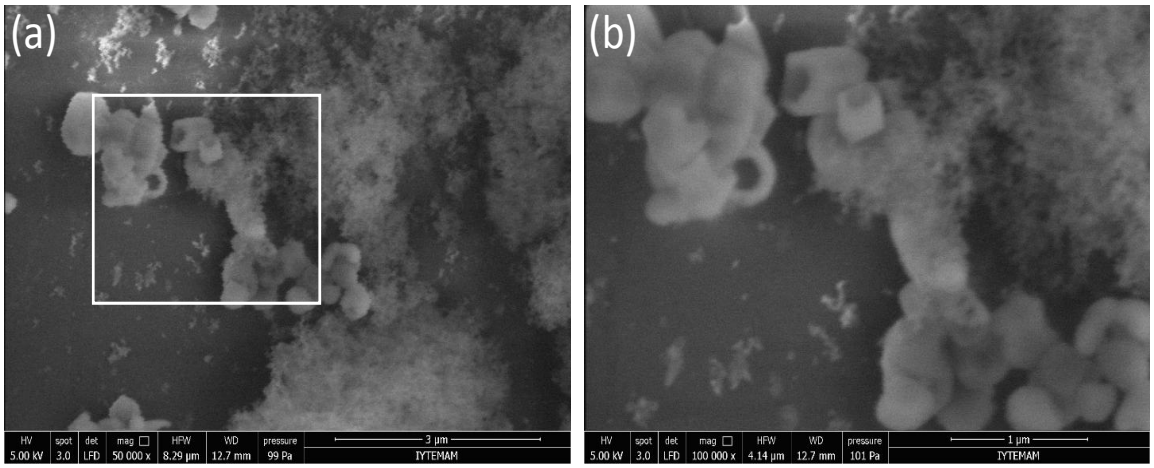

Figure 4.20. SEM images of hollow nano calcite particles mixed with fumed silica to form core material for a VIPs.

Figure 4.21 shows thermal conductivity values measured at different vacuum levels for the VIPs containing fumed silica and hollow nano calcite particles at different ratios. When the thermal conductivities of materials were examined, fumed silica was shown to be one of the best commercial core materials. As can be seen from the figure, the thermal conductivity for hollow calcite is higher than that for the fumed silica. The thermal conductivity values for other mixtures were also shown to be higher than that for the fumed silica. Unfortunately, hollow nano calcite was shown to be five times lower performance compared to the fumed silica in terms of thermal properties. On the other hand, the thermal conductivity of 3 wt% of hollow nano calcite in fumed silica showed lower thermal conductivity compared to the pure fumed silica. It seems that when hollow nano calcite particles were mixed with the fumed silica to certain amounts, much less thermal conductivity values can be obtained. Thermal conductivity of the VIP using the fumed silica as the core material was 9.9 $mWm^{-1}K^{-1}$, which decreased to 8.63 $mWm^{-1}K^{-1}$ when 3 wt% of hollow nano calcite particles were used in fumed silica.

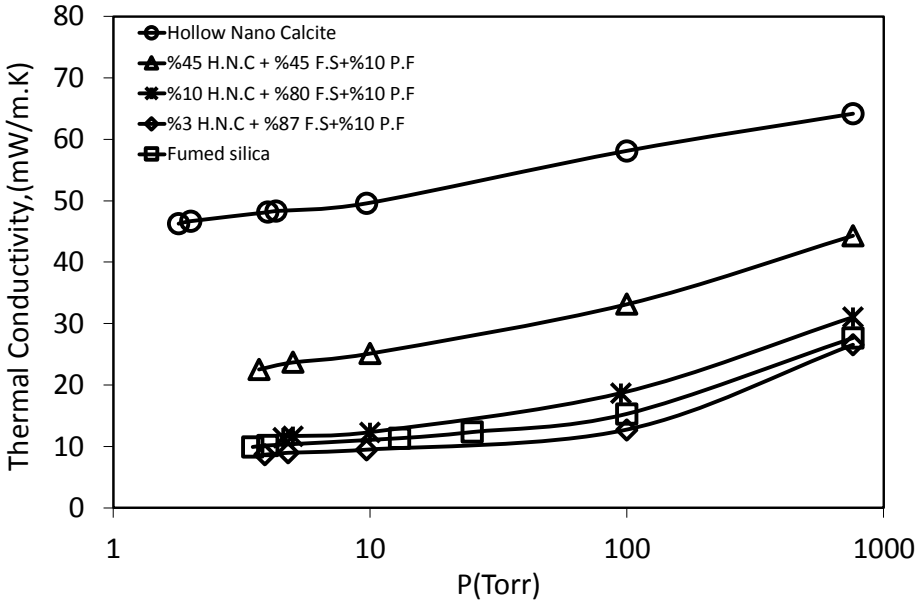

Figure 4.21. Thermal conductivity values measured at different vacuum levels for the VIPs containing fumed silica and hollow nano calcite particles at different ratios

Figure 4.22 shows the thermal conductivity of VIPs with core material containing different amount of hollow nano calcite particles in fumed silica, and the difference between the measured thermal conductivity and thermal conductivity of the mixture for the ideal mixture. As shown in Figure 4.22a, the measured thermal conductivity is always less than the conductivity calculated for the ideal mixture. The difference between the measured thermal conductivity and the ideal thermal conductivity of the mixture was about 5 $mWm^{-1}K^{-1}$. This difference may not be significant at higher hollow calcite contents in core material, however, it would be very important at lower hollow nano calcite contents in the core material of the VIPs. This is indeed one of the important findings in this thesis that better thermal conductivity values can be obtained when low amounts of hollow nano calcite particles were mixed with fumed silica as the core material in VIPs.

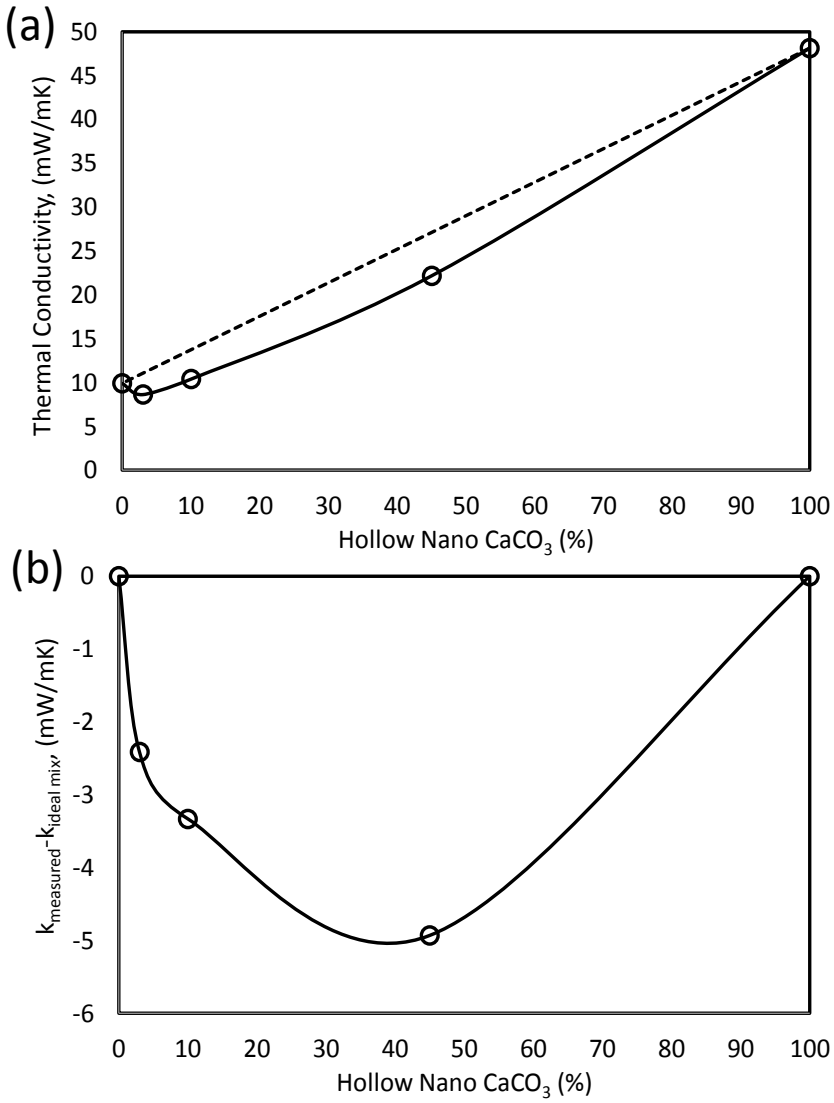

Figure 4.22. (a) Thermal conductivity of VIPs with core material containing different amount of hollow nano calcite particles in fumed silica, and (b) difference between the measured thermal conductivity and the ideal thermal conductivity of the mixture.

The thermal conductivities for hollow nano calcite and regular *Adacal*® nano calcite were measured and compared. The SEM images of *Adacal*® and hollow nano calcite particles were shown in Figure 4.23. As can be seen in the figure, the *Adacal*® calcite is almost homogenously distributed but they are filled particles. The *Adacal*® calcite is commercially available with sizes less than about 60 nm. These particles are smaller in size than the produced hollow nano calcite particles which were about 250 nm in size.

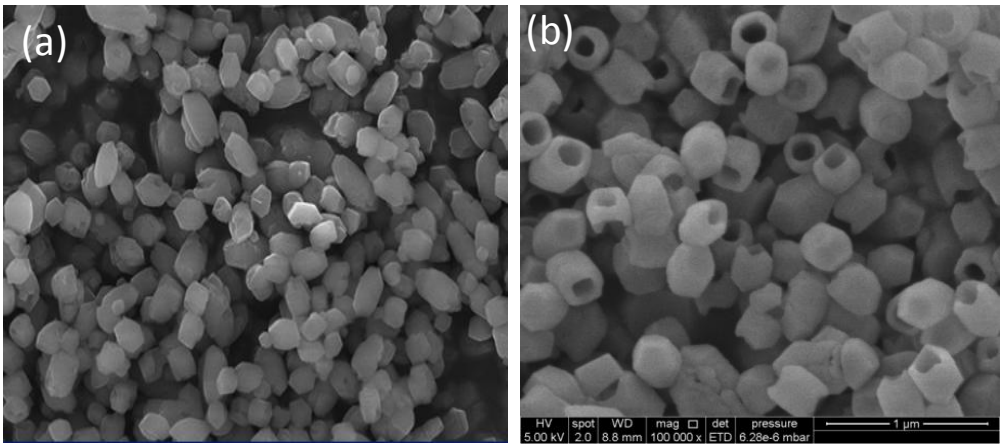

Figure 4.23. SEM image of (a) *Adacal*® nano calcite and (b) hollow nano calcite particles

Figure 4.24 shows thermal conductivity values for VIPs using hollow nano calcite and *Adacal*® nano calcite as the core material. Here, two calcite materials with similar physical properties, one is porous and the other is nonporous, were compared. As can be seen from the figure, the thermal conductivity for the hollow nano calcite is less than those for the *Adacal*® calcite at different vacuum pressures. It seems that the porosity is important to lower the thermal conductivity values. Hollow nano calcite has higher surface area, creates extra volume in the VIPs and therefore the hollow nano calcite is more advantageous compared to the *Adacal*® calcite.

Thermal conductivities of some other materials, which could be a candidate for the VIPs as core materials, were measured as shown in Table 4.1. The table shows the thickness of the VIP panels used in the measurements, the measured thermal conductivity values, the overall thermal conductivity values considering the thickness of the materials, and the packing density of the materials. As can be seen in the table, the lowest thermal conductivity value belongs to the fumed silica with about 9.9 $mWm^{-1}K^{-1}$. Hollow silica has thermal conductivity values of about 24 $mWm^{-1}K^{-1}$ and that for polyurethane foam is about 34 $mWm^{-1}K^{-1}$. Thermal conductivities for Plexiglas, polyethylene and derlin panels were measured to be about 170 $mWm^{-1}K^{-1}$ and considered to be high conducting materials.

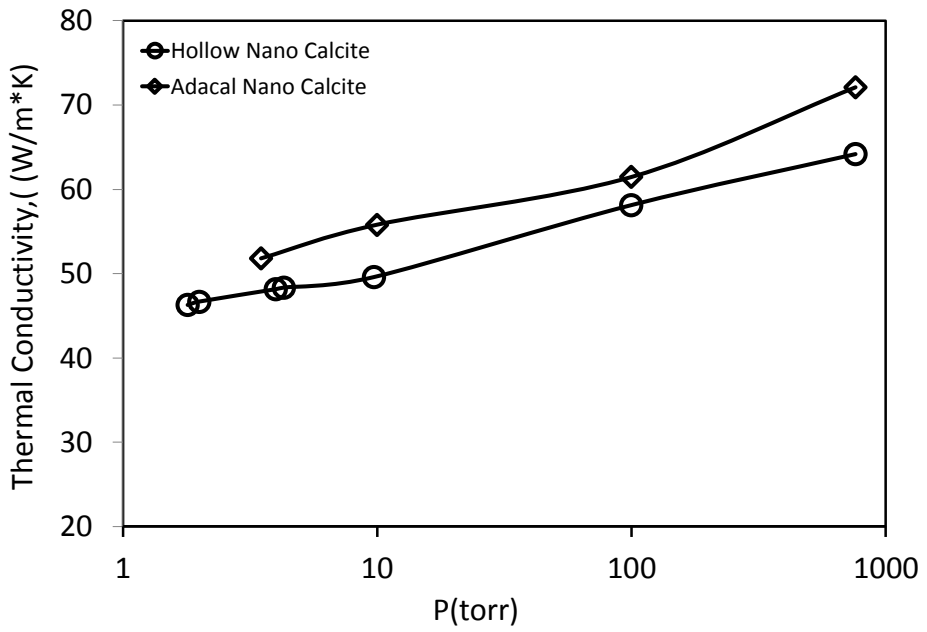

Figure 4.24. Thermal conductivity values for VIPs using hollow nano calcite and *Adacal*® nano calcite as the core material

Hollow nano calcite has thermal conductivity values of about 46 $mWm^{-1}K^{-1}$, which is better than expected. Pore diameters of hollow silica, hollow nano calcite, and fumed silica were measured approximately 300 nm, 40 nm and 10 nm, respectively. Packing density of these materials were measured as 200 kgm^{-3}, 660 kgm^{-3} and 175 kgm^{-3} as well. Although packing density of hollow silica and fumed silica are close to each other, there is striking differences in their conductivities. The hollow calcite, which has higher packing density, had a higher thermal conductivity compared to those for both silica's. Although all of these materials have a highest porous structure, fumed silica which has the largest surface area showed better thermal conductivity. On the other hand, the polyurethane foam has a packed density of about 60 kgm^{-3} and is the lightest weight of all, where fumed silica has 175 kgm^{-3}, which is close to the packing density of hollow silica of about 180 kgm^{-3}. These core materials make the VIPs lighter in weight with a low mechanical strength. The packing density of hollow nano calcite is about 667 kgm^{-3} and could be a better candidate with a higher mechanical strength.

Table 4.1.Measured thermal conductivity values for possible core materials for VIPs.

Materials	**Thickness (mm)**	**Thermal Conductivity (mW/m.K)**	**Overall Thermal Conductivity ($W/m^2.K$)**	**Density (kg/ m^3)**
Fumed silica	19.7	9.9	0.502	175.14
Hollow Nano Calcite	15.5	46,26	2.98	667.29
Adacal calcite	17.9	55.18	3.106	783.78
Hollow silica	14.6	24.67	1.69	180.04
Polystyrenefoam	28.7	40.5	1.411	14.6
Glass wool	34.2	36.87	0.936	76.8
XPS	18.0	37.68	2.088	28.24
HLM composite Panel	40.0	37.26	0.933	31.07
Polyurethane open cell	24.6	34.03	1.382	60.90
Polyurethane closed Surface	25.7	33.54	1.307	67.55
Plexyglass panel	14.3	164.19	11.572	-
PE panel	14.3	168.89	8.567	-
Delrin panel	24.9	190.59	9.345	-

CHAPTER 5

CONCLUSIONS

Hollow nano calcite particles were produced and employed in vacuum insulating materials (VIPs)as a core material. A fluidized bed filtration system was developed to separate the newly produced nano calcite particles and good results were obtained. Produced hollow nano-$CaCO_3$ particles were approximately 300 nm in size and with a pore size of about 40 nm. The thermal conductivity of the VIP prepared using the hollow nano calcite particles was measured to be 46 $mWm^{-1}K^{-1}$. This value was higher than the conductivity value of 9.9 $mWm^{-1}K^{-1}$ obtained for the VIP using the fumed silica, as the generally used core material. However, measurements have shown that thermal conductivities of the VIPs prepared with a mixture of hollow nano $CaCO_3$ and fumed silica were better. The thermal conductivity of VIP employing 3% hollow nano-$CaCO_3$ and 87% fumed silica as the core material was 8.63 $mWm^{-1}K^{-1}$, which was better than that of the VIP employing the fumed silica only.

The thermal conductivity of a VIP containing the *Adacal*® calcite as the core material was measured as 55 $mWm^{-1}K^{-1}$ and compared its performance with hollow nano-$CaCO_3$ for which the thermal conductivity was obtained to be about 46 $mWm^{-1}K^{-1}$. The thermal conductivity of the VIP was better for the hollow nano-$CaCO_3$ showing a significant pore effect in the VIPs.

Air and water vapor transfer rate are important in the life-time of a VIP. The outer protective layer of a VIP was coated with zinc-tin-oxide ($ZnSnO_x$) and measured the water vapor transmission rate. The envelope was PA/PE polymeric films and compared with the Al-PET which was known to be widely used in commercial market. The effects of wrapping rate as rpm and O_2 feed rate were investigated on the water vapor transfer rates through the $ZnSnO_x$ coated PA/PE films. It was found that while WVTR was measured to be 8.319 $gday^{-1}m^{-2}$ for the Al-PET, it was 1.1480 $gday^{-1}m^{-2}$ for the $ZnSnO_x$ coated PA/PE films of 90 μm, which was much better barrier property comparing to commercial Al-PET.

Although the thermal conductivity of a VIP obtained for the fumed silica is much advantageous, the packing density of the fumed silica, 175 kgm^{-3}, is much lower than the packing density of the hollow-nano calcite, 667 kgm^{-3}. The fumed silica may make the VIPs much lighter in weight but the mechanical strength may become lower. The packing density of hollow nano calcite is about 667 kgm^{-3} and could be a better candidate with a higher mechanical strength.

REFERENCES

Abe, H., I. Abe, K. Sato and M. Naito., 2005. "Dry powder processing of fibrous fumed silica compacts for thermal insulation." *Journal of the American Ceramic Society* 88(5), p. 1359-1361.

Al Omari, M., I. Rashid, N. Qinna, A. Jaber and A. Badwan., 2016. "Chapter Two-Calcium Carbonate." *Profiles of Drug Substances, Excipients and Related Methodology* 41, p. 31-132.

Alam, M., H. Singh and M. Limbachiya., 2011. "Vacuum Insulation Panels (VIPs) for building construction industry–A review of the contemporary developments and future directions." *Applied energy* 88(11), p. 3592-3602.

Alotaibi, S. S. and S. Riffat., 2014. "Vacuum insulated panels for sustainable buildings: a review of research and applications." *International Journal of Energy Research* 38(1), p. 1-19.

Andreassen, J.-P., 2001."Growth and aggregation phenomena in precipitation of calcium carbonate." *PhD. Dissertation*, Norwegian University of Science and Technology.

Araki, K., D. Kamoto and S.-i. Matsuoka., 2009. "Optimization about multilayer laminated film and getter device materials of vacuum insulation panel for using at high temperature." *Journal of materials processing technology* 209(1), p. 271-282.

Arita, Y., M. Mazilu and K. Dholakia., 2013. "Laser-induced rotation and cooling of a trapped microgyroscope in vacuum." *Nature communications* 4, p. 1-7.

Baetens, R., B. P. Jelle and A. Gustavsen., 2011. "Aerogel insulation for building applications: a state-of-the-art review." *Energy and Buildings* 43(4): 761-769.

Beikircher, T. and M. Demharter., 2013. "Heat Transport in Evacuated Perlite Powders for Super-Insulated Long-Term Storages up to 300 ˚C." *Journal of heat transfer* 135(5): 1-11.

Boafo, F. E., Z. Chen, C. Li, B. Li and T. Xu., 2014. "Structure of vacuum insulation panel in building system." *Energy and Buildings* 85, p. 644-653.

Bouquerel, M., T. Duforestel, D. Baillis and G. Rusaouen., 2012. "Mass transfer modeling in gas barrier envelopes for vacuum insulation panels: A review." *Energy and Buildings* 55, p. 903-920.

Brunner, S., P. Gasser, H. Simmler and K. G. Wakili., 2006. "Investigation of multilayered aluminium-coated polymer laminates by focused ion beam (FIB) etching." *Surface and Coatings Technology* 200(20), p. 5908-5914.

Caps, R. and J. Fricke., 2000. "Thermal conductivity of opacified powder filler materials for vacuum Insulations1." *International Journal of Thermophysics* 21(2), p. 445-452.

Caps, R., J. Fricke and H. Reiss., 1984. Improving the extinction properties of an evacuated high-temperature powder insulation. *European conference on thermophysical properties*. 15, p. 225-232..

Chan, C.-M., J. Wu, J.-X. Li and Y.-K. Cheung., 2002. "Polypropylene/calcium carbonate nanocomposites." *polymer* 43(10), p. 2981-2992.

Chang, M.-C. and C. Y. Tai., 2010. "Effect of the magnetic field on the growth rate of aragonite and the precipitation of $CaCO_3$." *Chemical Engineering Journal* 164(1), p. 1-9.

Chen, J. and L. Xiang., 2009. "Controllable synthesis of calcium carbonate polymorphs at different temperatures." *Powder Technology* 189(1), p. 64-69.

Di, X., Y. Gao, C. Bao and S. Ma., 2014. "Thermal insulation property and service life of vacuum insulation panels with glass fiber chopped strand as core materials." *Energy and Buildings* 73, p. 176-183.

Fahlteich, J., W. Schönberger, M. Fahland and N. Schiller., 2011. "Characterization of reactively sputtered permeation barrier materials on polymer substrates." *Surface and Coatings Technology* 205, p. 141-144.

Flaten, E. M., M. Seiersten and J.-P. Andreassen., 2009."Polymorphism and morphology of calcium carbonate precipitated in mixed solvents of ethylene glycol and water." *Journal of Crystal Growth* 311(13), p. 3533-3538.

Fricke, J., H. Schwab and U. Heinemann., 2006. "Vacuum insulation panels–exciting thermal properties and most challenging applications." *International journal of thermophysics* 27(4), p. 1123-1139.

Gao, F., 2012. *Advances in polymer nanocomposites: Types and applications*, Elsevier.

Garcí, J., J. G. Morales, J. F. Sáinz and E. Loste., 2004. "The mechanism of precipitation of chain-like calcite." *Journal of crystal growth* 262(1), p. 479-489.

García-Carmona, J., J. G. Morales and R. R. g. Clemente., 2003. "Morphological control of precipitated calcite obtained by adjusting the electrical conductivity in the Ca $(OH)_2$–H_2O–CO_2 system." *Journal of crystal growth* 249(3), p. 561-571.

Guo, H., J. Yu and B. Cheng., 2006. "Preparation and formation mechanism of wood-block-like calcite particles." *Journal of Solid State Chemistry* 179(8), p. 2547-2553.

Hadiko, G., Y. S. Han, M. Fuji and M. Takahashi., 2005. "Synthesis of hollow calcium carbonate particles by the bubble templating method." *Materials Letters* 59(19), p. 2519-2522.

Han, Y. S., G. Hadiko, M. Fuji and M. Takahashi., 2006. "Crystallization and transformation of vaterite at controlled pH." *Journal of crystal growth* 289(1), p. 269-274.

Heineman, U., H. Schwab, H. Simmler, S. Brunner, K. Ghazi, R. Bundi, K. Kumaran, P. Mukhopadhyaya, D. Quénard and H. Sallée., 2005. "Vacuum insulation." *Panel properties and building applications (summary), Final report for the IEA/ECBCS Annex* 39.

Henry, B., A. Erlat, A. McGuigan, C. Grovenor, G. Briggs, Y. Tsukahara, T. Miyamoto, N. Noguchi and T. Niijima., 2001. "Characterization of transparent aluminium oxide and indium tin oxide layers on polymer substrates." *Thin Solid Films* 382(1), p. 194-201.

Hu, L., P. Dong and G. Zhen., 2009. "Preparation of active $CaCO_3$ nanoparticles and mechanical properties of the composite materials." *Materials Letters* 63(3), p. 373-375.

Jung, H., I. Yeo and T.-H. Song., 2014. "Al-foil-bonded enveloping and double enveloping for application to vacuum insulation panels." *Energy and Buildings* 84, p. 595-606.

Kaganer, M. G., 1969. *Thermal insulation in cryogenic engineering*, Israel Program for Scientific Translations.

Karami, P., E. T. Afriyie, P. Norberg and K. Gudmundsson., 2014. "A study of the thermal conductivity of granular silica materials for VIPs at different levels of gaseous pressure and external loads." *Energy and Buildings* 85, p. 199-211.

Kim, J., J.-H. Lee and T.-H. Song., 2012. "Vacuum insulation properties of phenolic foam." *International Journal of Heat and Mass Transfer* 55(19), p. 5343-5349.

Kistler, S. and A. Caldwell., 1934. "Thermal conductivity of silica aerogel." *Industrial & Engineering Chemistry* 26(6), p. 658-662.

Konno, H., Y. Nanri and M. Kitamura., 2003. "Effect of NaOH on aragonite precipitation in batch and continuous crystallization in causticizing reaction." *Powder technology* 129(1), p. 15-21.

Kralj, D., L. Brečević and J. Kontrec., 1997. "Vaterite growth and dissolution in aqueous solution III. Kinetics of transformation." *Journal of crystal growth* 177(3), p. 248-257.

Kwon, J.-S., C. H. Jang, H. Jung and T.-H. Song., 2009. "Effective thermal conductivity of various filling materials for vacuum insulation panels." *International Journal of Heat and Mass Transfer* 52(23), p. 5525-5532.

Kwon, J.-S., C. H. Jang, H. Jung and T.-H. Song., 2010. "Vacuum maintenance in vacuum insulation panels exemplified with a staggered beam VIP." *Energy and Buildings* 42(5), p. 590-597.

Li, C.-D., Z.-C. Duan, Q. Chen, Z.-F. Chen, F. E. Boafo, W.-P. Wu and J.-M. Zhou., 2013. "The effect of drying condition of glassfibre core material on the thermal conductivity of vacuum insulation panel." *Materials & Design* 50, p. 1030-1037.

Liang, J., 2007. "Evaluation of dispersion of nano-$CaCO_3$ particles in polypropylene matrix based on fractal method." *Composites Part A: Applied Science and Manufacturing* 38(6), p. 1502-1506.

Lin, Y., H. Chen, C.-M. Chan and J. Wu., 2008. "High impact toughness polypropylene/$CaCO_3$ nanocomposites and the toughening mechanism." *Macromolecules* 41(23), p. 9204-9213.

Lopez, O., P. Zuddas and D. Faivre., 2009. "The influence of temperature and seawater composition on calcite crystal growth mechanisms and kinetics: Implications for Mg incorporation in calcite lattice." *Geochimica et Cosmochimica Acta* 73(2): 337-347.

Lucas-Girot, A., M. C. Verdier, O. Tribut, J. C. Sangleboeuf, H. Allain and H. Oudadesse., 2005. "Gentamicin-loaded calcium carbonate materials: Comparison of two drug-loading modes." *Journal of Biomedical Materials Research Part B: Applied Biomaterials* 73(1), p. 164-170.

Marouani, S., 2012. "Investigation of the resistance welding of multilayers aluminum-coated polymer complexes used as envelopes of vacuum insulation panels." *Materials & Design* 36, p. 546-556.

Mukhopadhyaya, P., M. K. Kumaran, N. Normandin, D. van Reenen and J. Lackey., 2009. *Fibre-powder composite as core material for vacuum insulation panel*. 9th international vacuum insulation symposium, London, UK.

Nemanič, V., B. Zajec, M. Žumer, N. Figar, M. Kavšek and I. Mihelič., 2014. "Synthesis and characterization of melamine–formaldehyde rigid foams for vacuum thermal insulation." *Applied Energy* 114, p. 320-326.

Nemanič, V. and M. Žumer., 2015. "New organic fiber-based core material for vacuum thermal insulation." *Energy and Buildings* 90, p. 137-141.

Pontoni, D., J. Bolze, N. Dingenouts, T. Narayanan and M. Ballauff., 2003. "Crystallization of calcium carbonate observed in-situ by combined small-and wide-angle X-ray scattering." *The Journal of Physical Chemistry B* 107(22), p. 5123-5125.

Render, D., T. Samuel, H. King, M. Vig, S. Jeelani, R. J. Babu and V. Rangari., 2016. "Biomaterial-Derived Calcium Carbonate Nanoparticles for Enteric Drug Delivery." *Journal of Nanomaterials* 2016, p. 1-8

Rieger, J., J. Thieme and C. Schmidt., 2000. "Study of precipitation reactions by X-ray microscopy: $CaCO_3$ precipitation and the effect of polycarboxylates." *Langmuir* 16(22), p. 8300-8305.

Sato, Y., J. Kiyohara, A. Hasegawa, T. Hattori, M. Ishida, N. Hamada, N. Oka and Y. Shigesato., 2009. "Study on inverse spinel zinc stannate, Zn_2SnO_4, as transparent conductive films deposited by rf magnetron sputtering." *Thin Solid Films* 518(4), p. 1304-1308.

Simmler, H. and S. Brunner., 2005. "Vacuum insulation panels for building application: Basic properties, aging mechanisms and service life." *Energy and Buildings* 37(11), p. 1122-1131.

Swimm, K., G. Reichenauer, S. Vidi and H.-P. Ebert., 2009. "Gas pressure dependence of the heat transport in porous solids with pores smaller than 10 μm." *International Journal of Thermophysics* 30(4), p. 1329-1342.

Tenpierik, M. J. and J. J. Cauberg., 2010. "Encapsulated vacuum insulation panels: Theoretical thermal optimization." *Building Research & Information* 38(6), p. 660-669.

Tseng, P. and H. Chu., 2009. "The effects of PE additive on the performance of polystyrene vacuum insulation panels." *International Journal of Heat and Mass Transfer* 52(13), p. 3084-3090.

Uebo, K., R. Yamazaki and K. Yoshida., 1992. "Precipitation mechanism of calcium carbonate fine particles in a three-phase reactor." *Advanced Powder Technology* 3(1): 71-79.

Ukrainczyk, M., J. Kontrec, V. Babić-Ivančić, L. Brečević and D. Kralj., 2007. "Experimental design approach to calcium carbonate precipitation in a semicontinuous process." *Powder technology* 171(3), p. 192-199.

Van Malsen, J., M. Tenpierik, R. Looman and J. Cauberg., 2008. "Heat Seal Strength of Barrier Films Used in Vacuum Insulation Panels At Room Temperature and At-130° C." *Journal of Plastic Film and Sheeting* 24(1), p. 35-52.

Wang, X., N. Walliman, R. Ogden and C. Kendrick., 2007. "VIP and their applications in buildings: a review." *Proceedings of the Institution of Civil Engineers-Construction Materials* 160(4), p. 145-153.

Willems, M., K. Schild and G. Hellinger., 2005. *Numerical investigation on thermal bridge effects in vacuum insulating elements*. Proceedings of the 7th international vacuum insulation symposium.

Willems, W. M., 2005. "The next generation of insulating materials: vacuum insulation."

Wray, J. L. and F. Daniels., 1957. "Precipitation of calcite and aragonite." *Journal of the American Chemical Society* 79(9), p. 2031-2034.